Development of crescentic bars for a periodically perturbed initial bathymetry

Meinard C. H. Tiessen,[1,2] Nicholas Dodd,[1] and Roland Garnier[3,4]

Received 22 April 2011; revised 29 July 2011; accepted 1 August 2011; published 2 November 2011.

[1] The development of crescentic bed patterns starting from an 'undisturbed' beach (i.e. one only perturbed so as to simulate background noise and thereby initiate morphological development) is compared with that starting from a beach where monochromatic (and in some cases bichromatic) bed patterns pre-exist, using a fully non-linear model (Morfo55). A wide range of different lengthscales and amplitudes is investigated. The findings suggest that the pre-existence of crescentic bed-forms can influence the subsequent morphological development of this beach significantly, but that this development is related to the undisturbed beach development. Whether a pre-existing bed-form remains under certain forcing conditions depends on the position of the pre-existing lengthscale along the undisturbed linear growth rate curve: If the pre-existing mode shows significant linear growth in the undisturbed scenario, this pre-existing lengthscale remains. Otherwise the pre-existing mode will be replaced by a bed-form with a lengthscale closer to the undisturbed fastest growing mode. A pre-existing lengthscale that is significantly longer than the undisturbed fastest growing mode will be replaced by a higher harmonic of the original lengthscale; for shorter pre-existing lengthscales, this will be the linear fastest growing mode. An increased amplitude of the pre-existing bed-form accelerates the development toward a new stable situation. For small initial amplitudes, the initial response of the system to pre-existing bed-forms could theoretically be described using linearized equations alone. The migration rates of both the pre-existing and newly arising modes correspond to the migration rate of these modes in the undisturbed scenario.

Citation: Tiessen, M. C. H., N. Dodd, and R. Garnier (2011), Development of crescentic bars for a periodically perturbed initial bathymetry, *J. Geophys. Res.*, *116*, F04016, doi:10.1029/2011JF002069.

1. Introduction

[2] Many beaches around the world display alongshore bars at a distance from the shoreline [*van Enckevort and Ruessink*, 2003]. Under certain conditions, these bars can deform into lunate shaped bed-forms [*Wright and Short*, 1984], called crescentic bars.

[3] Development of crescentic bed patterns generally occurs under moderate wave conditions. During storms, crescentic bars are (similar to other three dimensional bed-forms) erased, and only two dimensional bed-forms, like alongshore bars remain [*van Enckevort et al.*, 2004]. When wave conditions settle down, new bed patterns start to form. The alongshore lengthscale of crescentic bed patterns is dependent on a wide array of different circumstances. Increased wave heights and/or with more oblique waves generally result in longer spacings of bed-forms (i.e. lengthscales) than more moderate conditions [*van Enckevort et al.*, 2004; *Gallop et al.*, 2011]. However, also the underlying bathymetry (i.e. the cross-shore profile) influences the lengthscale of these bed-forms significantly [*Calvete et al.*, 2007]. Observed bed patterns generally have lengthscales between 200 and 500 m [*Komar and Holman*, 1986], although bed patterns with lengths of the order of 1000 m have also been observed [*van Enckevort et al.*, 2004; *Arifin and Kennedy*, 2011].

[4] In the past, it was assumed that circulation patterns and bed-forms in the nearshore zone were the result of a forcing template in the wave conditions [*Bowen and Guza*, 1978; *Holman and Bowen*, 1982; *Komar*, 1998]. Current understanding suggests, however, that the driving force behind the formation of bed-forms in the surf zone and the accompanying circulation patterns is, at least in the absence of directional spreading of the incoming waves, due to the evolution of free instabilities in the coastal system [*Hino*, 1974] (see *Reniers et al.* [2004] for results that suggest forced development as a result of directional spreading). Self-organization of the morphodynamical system, i.e., waves, currents, sediment transport, erosion and accretion, gives rise to the

[1]Faculty of Engineering, University of Nottingham, Nottingham, UK.
[2]Now at Royal Netherlands Institute for Sea Research, Texel, Netherlands.
[3]Departmento de Física Aplicada, Universitat Politécnica de Catalunya, Barcelona, Spain.
[4]Now at Instituto de Hidraulica Ambiental, Universidad de Cantabria, ETSI Caminos Canales y Puertos, Santander, Spain.

0148-0227/11/2011JF002069

development of a wide range of bed-forms, depending on the local conditions [*Coco and Murray*, 2007].

[5] Past numerical and theoretical studies have focused on both the initial and longer-term development of crescentic bed-forms, but only starting from an alongshore constant beach profile, and only perturbed by small perturbations to initiate bed pattern development [e.g., *Calvete et al.*, 2005; *Klein and Schuttelaars*, 2005; *Smit et al.*, 2008; *Garnier et al.*, 2008]. In reality, most three dimensional bed-forms are only substantially removed from a beach during storms [*van Enckevort et al.*, 2004; *Arifin and Kennedy*, 2011; *Gallop et al.*, 2011]; in between storms they persist. These prolonged durations when bed patterns exist at finite amplitude, during changing wave conditions, have only recently been investigated using process-based models. Rhythmically perturbed initial bathymetries have been used before [*Damgaard et al.*, 2002; *Klein and Schuttelaars*, 2006; *Castelle et al.*, 2010] but these investigations have focused on processes other than the impact of such initial features on the development of bed-forms. *Castelle et al.* [2010] and *Klein and Schuttelaars* [2006] used an initially perturbed bathymetry on a double barred beach to study the potential interaction and coupling of bed-forms.

[6] More recently, the impact of a change in the forcing conditions on the development of crescentic bed-forms has been studied. In pioneering work, *Smit* [2010] investigated to what extent the average lengthscale of crescentic bed-forms changed when two separate wave conditions were applied in series. The first wave conditions give rise to one morphological pattern (starting from an alongshore constant beach profile, with small random perturbations superimposed); the second set of wave conditions (starting from the same state) would result in a distinctly different bed pattern. Results of *Smit* [2010] show a clear change of the dominant lengthscale in some cases, but in others the initially developed bed-forms remain dominant. This behavior was found to be partially related to the duration before the wave conditions changed: A longer duration resulted in a bed-form that was less likely to change. However, these runs only lasted 20 days in total, and the increased duration of the initial wave conditions, therefore, caused a reduced duration over which the subsequent wave conditions were applied. The time it takes a bed-form to reach its fully developed state after a storm can be up to 3 weeks [*van Enckevort et al.*, 2004], but whether the development of crescentic bed-forms presented by *Smit* [2010] reaches a stable final height within the 20-day model runs is unknown. Furthermore, the initial development of crescentic bed-forms starts from a randomly perturbed bathymetry resulting in the development of an array of different lengthscales. As *Smit* [2010] only presents the temporal evolution of a weighted-averaged lengthscale across the domain, the extent to which different pre-existing lengthscales show different behavior also remains unknown.

[7] In the last decade, work on understanding the physics of the formation of morphodynamical features such as crescentic bed patterns has yielded insights into the growth and kinematics of these bed-forms. The use of a specific type of self-organization model, the stability analysis, in particular, has furthered our understanding of these bed patterns (see *Blondeaux* [2001], *Dodd et al.* [2003], *Coco and Murray* [2007], and *Falqués et al.* [2008] for several reviews on this topic).

[8] Recently, a linear stability analysis was tested under real-world circumstances; predictions made by such a model of the crescentic bed pattern lengthscale were compared with field observations [*Tiessen et al.*, 2010]. Several limitations are intrinsic to this modeling technique, which limit the applicability in the field, notably the linearized description of the bed pattern perturbations, and the assumption of alongshore uniformity. The initial development of crescentic bed patterns, as described by a linear stability analysis, only occurs in reality immediately after a storm, when all pre-existing bed-forms are wiped out, and a quasi-constant alongshore beach profile exists. The development of crescentic bed-forms under one set of forcing conditions immediately after a storm (when a quasi-alongshore beach exists) can in general not be assumed to be the same as the bed pattern development under the same forcing conditions, when, in between storms, bed-forms are already present. A non-linear numerical model is used here to investigate the development of crescentic bed patterns over longer periods of time and in the presence of pre-existing bed-forms. This modeling technique has been applied extensively in recent years, also to further investigate the physics behind these bed-forms [*Caballeria et al.*, 2002; *Damgaard et al.*, 2002; *Klein*, 2006; *Coco and Murray*, 2007; *Garnier et al.*, 2008; *Smit et al.*, 2008; *Garnier et al.*, 2010].

[9] The present study investigates a wide range of monochromatic pre-existing bed pattern lengthscales to identify mechanisms by which some bed-forms may grow and others decay, and quantify the effect this can have on the subsequent development of crescentic bed-forms. This is obscured from more general analyses, when a wider array of pre-existing bed-forms is present. This research thus aims to provide an explanation of the mechanisms by which crescentic bed-forms develop (or not) from pre-existing crescentic-type morphologies. The present study also provides a comparison between the development when bed patterns already exist at the start of the model run, and that of crescentic bed patterns starting from an alongshore constant beach profile, only perturbed by a 0.03 m high "spike" in the middle of the modeled domain (a numerical analogue of a Dirac-delta function (previously used by *Garnier et al.* [2006]) to initiate bed pattern development. The initial stages of this "undisturbed" development, correspond with what would be predicted by a linear stability analysis. Additionally, therefore, we also address the question of to what extent linear stability analysis can be used to describe the development of crescentic bed-forms, when these bed patterns already exist. In order to investigate the response of the system to pre-existing bed-forms, a method is used, where the overall bathymetric evolution is dissected into different modes using a Fourier analysis (a similar method has previously been used by *Klein and Schuttelaars* [2006]). The development of different modes is subsequently analyzed to identify the impacts of different pre-existing bed-pattern amplitudes ($A_{\text{ini.}}$) and lengthscales ($\lambda_{\text{ini.}}$). This method enables us to identify not only global characteristics, such as the amplitude (A_{final}) and lengthscale of the final topography (λ_{final}) and the duration before a new stable situation has established (denoted here as the 'development time'; note that this is not the same as the *e*-folding time), but also separate characteristics of both the pre-existing and finally dominant mode. The amplitude development of both $\lambda_{\text{ini.}}$ and λ_{final} can be derived, along

with migration rates of either mode. Furthermore the extent to which the initial responses of the system of pre-existing bed-forms still corresponds to the predictions made by a linear stability analysis can be investigated.

[10] In the following section a brief introduction to the model as well as the model settings and the research set-up is presented. Afterwards the development of crescentic bed patterns from an alongshore constant beach profile is presented, along with an introduction of the methods used to identify different processes and characteristics in order to quantify and differentiate between various responses of the nearshore zone system. Then the undisturbed development is compared to the response of the nearshore bathymetry, when bed patterns pre-exist. Subsequently, we provide an investigation into the impact of various initial pre-existing lengthscales and amplitudes on the development of crescentic bed-forms. The effects of different pre-existing crescentic bed patterns on various different characteristic lengthscales, amplitudes, linear growth rates and migration rates are examined. Thereafter, the implications that pre-existing bed-forms can have on subsequent crescentic bed pattern development are related to field observations. Finally, a discussion is presented and conclusions are drawn.

2. Methodology

2.1. Model Equations

[11] Morfo55 is a fully non-linear time domain model that describes morphological developments in the nearshore zone (see *Caballeria et al.* [2002] and *Garnier et al.* [2006] for more details). The model uses depth- and wave-averaged equations along with a wave energy equation to describe nearshore hydrodynamics [*Mei*, 1990]. To couple the bed evolution with the hydrodynamics a sediment mass conservation equation is used. Combined, this results in the following set of equations:

$$\frac{\partial D}{\partial t} + \frac{\partial}{\partial x_j}\left(D v_j\right) = 0, \tag{1}$$

$$\frac{\partial v_i}{\partial t} + v_j \frac{\partial v_i}{\partial x_j} = -g\frac{\partial z_s}{\partial x_i} - \frac{1}{\rho D}\frac{\partial}{\partial x_j}\left(S'_{ij} - S''_{ij}\right) - \frac{\tau_{bi}}{\rho D}, \tag{2}$$

$$\frac{\partial E}{\partial t} + \frac{\partial}{\partial x_i}\left(\left(v_i + c_{gi}\right)E\right) + S'_{ij}\frac{\partial v_j}{\partial x_i} = -\mathcal{D}, \tag{3}$$

$$\vec{\nabla} \times \vec{\kappa} = 0, \tag{4}$$

$$\frac{\partial z_b}{\partial t} + \frac{1}{1-p}\frac{\partial q_i}{\partial x_i} = 0 \tag{5}$$

where $i, j = 1, 2$, $\overrightarrow{x} = (x_1, x_2) = (x, y)$ and $\overrightarrow{v} = (v_1, v_2) = (u, v)$. x and y are the cross- and alongshore coordinates, and u and v the cross- and alongshore depth-averaged velocities, respectively. z_s is the mean sea level, z_b the mean bed level, D the total mean water depth ($D = z_s - z_b$), and c_{g_i} are the components of the wave group velocity vector [see, e.g., *Mei*, 1990]. $\overrightarrow{\tau_b}$ represents bed shear stress ($\overrightarrow{\tau_b} = (\tau_{b_1}, \tau_{b_2}) = (\tau_{b_x}, \tau_{b_y})$), which is represented as linear friction, such that the depth-averaged current is small compared to the wave orbital velocity at the edge of the boundary layer.

[12] S'_{ij} is the radiation stress term [*Longuet-Higgins and Stewart*, 1964] and S''_{ij} represents the Reynolds stresses. The *Battjes* [1975] model is used to describe the horizontal eddy viscosity (ν_t).

[13] $\mathcal{D}$ describes the loss of wave energy due to wave breaking [*Thornton and Guza*, 1983].

[14] The wave angle is given using equation (4) where $\vec{\kappa} = (\kappa_1, \kappa_2) = (\kappa_x, \kappa_y)$ can be computed using the dispersion relation [*Mei*, 1990]:

$$\sigma^2 = g\,\kappa\,\tanh(\kappa D),$$

where σ is the intrinsic wave frequency, i.e., that observed when moving with the current ($\vec{v}$). The relation between σ and the absolute frequency ω_w is given by [*Svendsen*, 2006]:

$$\omega_w = \sigma + v_j\kappa_j.$$

[15] The sediment flux is $\overrightarrow{q}$ ($\overrightarrow{q} = (q_1, q_2) = (q_x, q_y)$), where p is porosity of the sediment. Here we take the Soulsby and Van Rijn [*Soulsby*, 1997] total load formula ($\overrightarrow{q}$) and augment it with a down-slope diffusion term, so that

$$\overrightarrow{q} = \alpha\left(\overrightarrow{v} - \gamma u_b \overrightarrow{\nabla} h\right), \tag{6}$$

where α is a stirring function, γ is the down-slope bed diffusion coefficient, u_b is the root mean square wave orbital velocity at the seabed and h is the bed level deviation from the initial undisturbed equilibrium profile (for more details see *Garnier et al.* [2006]).

[16] To what extent bed-forms experience down-slope movement of sediment under gravity is dependent on the down-slope term (γ). For the modeling of field conditions, a value of 1.6 [m^2/s] is generally used (for instance, by *Tiessen et al.* [2010]). However, in order also to investigate the impacts of pre-existing lengthscales that show linear decay, an increased down-slope term ($\gamma = 5$ [m^2/s]) is used in this research (previously used by *Garnier et al.* [2008]). The impact of this increased down-slope term is further discussed in section 6. Model settings, and general information concerning the presented model runs are shown in Table 1.

2.2. Numerical Solution

[17] The Morfo55 model uses a finite difference scheme to discretize the basic governing equations. A central finite difference method on a regular rectangular grid is used for the spatial derivatives. The grid distribution is set at $\Delta x =$ 2.5 m and $\Delta y = 10$ m, to ensure convergence for $\lambda \geq 100$ m. The explicit Adams–Bashforth scheme is used for temporal derivatives. In order to accelerate morphological processes, a morphological acceleration factor of 60 has been applied to the hydrodynamical time step, resulting in a morphological time step of 3 s (see *Caballeria et al.* [2002] and *Garnier et al.* [2006] for more details). Sensitivity of the model results for different values of the morphological acceleration factor (c_{moac}) has been investigated, and was found to be negligible. The alongshore domain length (L_y)

Table 1. Parametrization of the Terms Used in the Morfo55 Runs

Name	Parameter	Unit	Value
General			
Gravitational acceleration	g	m/s^2	9.8
Offshore boundary	L_x	m	250
Alongshore domain width	L_y	m	2000
Minimum bed level at shoreline	$z_{\min}$	m	0.25
Range of examined lengthscales	λ	m	100–1000
Morphological acceleration coefficient	c_{moac}	–	60
Morphological time step	δt_m	s	3.0
Dissipation[a]			
Coefficient of wave dissipation	B^3	–	1.0
Breaking index	γ_b	–	0.6
Reynolds Stresses[b]			
Turbulence parameter	M	–	1.0
Friction[c]			
Bottom friction coefficient	c_d	–	0.01 (constant)
Sediment[d]			
Median grain size	d_{50}	m	2.5×10^{-4}
Bed roughness length	z_{rl}	m	0.01
Kinematic viscosity	μ	m^2/s^2	1.3×10^{-6}
Sediment porosity	p	–	0.4
Relative sediment density	s_{rds}	–	2.65
Bedslope coefficient	γ	m^2/s	5

[a]According to *Thornton and Guza* [1983].
[b]According to *Battjes* [1975].
[c]Linear friction is applied [*Calvete et al.*, 2005].
[d]Sediment transport according to *Soulsby* [1997].

is 2000 m, with periodic lateral boundaries. Longer alongshore domain widths produce no significant difference to results. The offshore boundary is at $x = 250$ m ($D(x = 250\text{ m}) = 4.5$ m), where the wave conditions are imposed. z_s and z_b are free, and u and v decay exponentially. At the shoreward boundary a minimum depth (0.25 m) is applied, and u, v and q_x set to zero; other variables are free.

2.3. Research Set-Up

[18] To compare undisturbed development of crescentic bed-forms with that when this type of bed pattern already exists, idealized circumstances are created. Constant forcing conditions are applied at the offshore boundary. Normal and oblique ($\theta = 5°$) wave incidence are applied, with moderate wave height ($H_{rms} = 0.9$ m), and period $T_p = 7.5$ s. These conditions correspond roughly to moderate wave conditions that occur in between storms at Duck (North Carolina, USA), and give rise to the development of crescentic bed-forms there [*van Enckevort et al.*, 2004]. Generally, only oblique wave incidence results are presented here (normal wave incidence results confirm findings for the oblique case).

[19] The alongshore constant beach profile is based on the beach profile at Duck of *Yu and Slinn* [2003]. Here, this beach is perturbed by an "infinitesimal" perturbation to initiate bed pattern development, a numerical analogue of a Dirac-delta function [*Garnier et al.*, 2006]. This 'Dirac function' is a spike of 0.03 m height in the seabed, at 50 m offshore in the center of the domain. This spike excites a wide range of lengthscales equally, allowing initial development of all these bed-forms. Hereafter we refer to these experiments as the "undisturbed" development of crescentic bed-forms, since no specific pre-existing bed patterns are present at the start of the run.

2.4. Pre-Existing Modes

[20] To examine development from pre-existing bed patterns finite-amplitude, periodic perturbations are superimposed on the alongshore constant beach. A wide array of different initial lengthscales ($\lambda_{\text{ini.}}$) is tested, corresponding to various harmonics of L_y ($\lambda_{\text{ini.}} = 100, 111, 133, 166, 200, 250, 286, 333, 400, 500, 666, 1000$ m). Pre-existing bed patterns are given three different initial amplitudes ($A_{\text{ini.}} = 0.05, 0.15, 0.25$ m). These amplitudes are chosen approximately to span the linear growth domain so that the smallest amplitude may be expected to evolve linearly (under the present forcing conditions), whereas the largest amplitude might be expected to behave non-linearly. Note that in this case, no 'Dirac function' is imposed, only the pre-existing modes. These pre-existing bed-forms are computed using results from a linear stability analysis (Morfo60, [*Calvete et al.*, 2005]). This model gives a description of the initial development of each examined lengthscale, resulting in a monochromatic description of the seabed at the start of a model run of each examined pre-existing lengthscale. Thus all pre-existing modes are linear solutions. Their cross-shore appearance therefore varies with lengthscale, however this variation is limited.

[21] The linear stability model settings closely correspond with the settings used in the non-linear model runs (when starting from an alongshore constant beach). However, to construct these pre-existing bed-forms we consider a larger wave height ($H_{rms} = 1.3$ m) and decreased value for γ (1.6 m^2/s) than that used for the subsequent analysis (previously stated as $H_{rms} = 0.9$ m, $\gamma = 5$ m^2/s). The reason for this is twofold: i) to approximate the pre-existing development of bed-forms as wave heights gradually settle post-storm: the pre-existing bed-forms originate from slightly more energetic forcing conditions after the storm, while the moderate wave conditions that occur in between storms govern the bathymetric response (as is modeled by the non-linear model); and ii) to allow the examination of morphological development for pre-existing bed-forms whose wavelengths correspond to a decaying linear mode under the new wave conditions ($H_{rms} = 0.9$ m): see Figure 1. Note that we do not alter the wave period ($T_p = 7.5$ s). This discrepancy in the wave height results in a slight offshore displacement of the pre-existing bed-forms, compared to their location under the more moderate conditions applied during the Morfo55 runs. Indeed, crescentic bed pattern formation is linked to the cross-shore distribution of the depth-averaged sediment concentration [*Falqués et al.*, 2000], which largely depends on the wave orbital-velocity. The position of its maximum controls the initial location of the rhythmic patterns. A shift in forcing conditions, can therefore cause a shift in optimum bed pattern location [*Garnier et al.*, 2010].

[22] This shoreward shift occurs within a brief period at the start of each model run (within 2 days), when the wave conditions are still being ramped up, causing the pre-existing bed-forms to be located at the optimum location for crescentic bed pattern development after this time. This initial shift in cross-shore location of pre-existing crescentic bed-

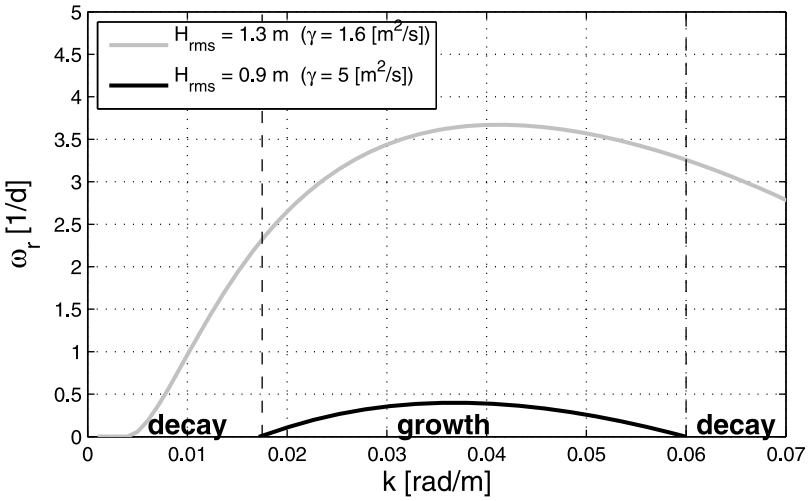

Figure 1. Linear growth rate for various crescentic bed pattern lengthscales ($k = \frac{2\pi}{\lambda}$ [rad/m]) for the conditions used to create the pre-existing bed-forms (H_{rms} = 1.3 m, T_p = 7.5 s, $\theta = 0°$, γ = 1.6 [m^2/s]), and those used to describe subsequent development of crescentic bed patterns (H_{rms} = 0.9 m, T_p = 7.5 s, $\theta = 0°$, γ = 5 [m^2/s]), the latter also showing regions where lengthscales decay.

forms has no significant impact on subsequent morphological development.

[23] For all runs a Fourier analysis is carried out to determine the dominant lengthscale from the output of Morfo55. One alongshore transect is chosen for this purpose, and therefore represents the overall development of the bathymetry; a similar approach was used by *Garnier et al.* [2006]. This transect is at 50 m offshore, and lies just shoreward of the peak of the alongshore bar, where the 'Dirac function' is located in the undisturbed scenario.

3. Undisturbed Evolution of Crescentic Bed Patterns

[24] The evolution of the undisturbed seabed is shown in Figure 2, in which $A_\lambda \equiv A(\lambda)$, the amplitude of the Fourier

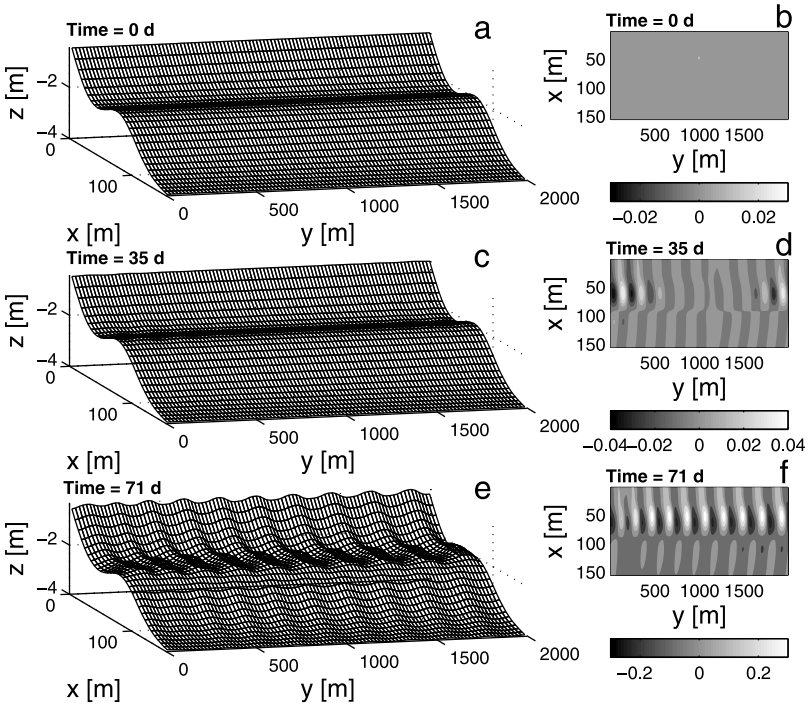

Figure 2. Evolution of the undisturbed nearshore bathymetry under oblique wave incidence ($\theta = 5°$). (a, b) Bed profile at beginning of model run. (c, d) Development of bed-forms after 35 days. (e, f) Bed patterns near the end of model run. Three dimensional view of the bed level (z_b) is shown in Figures 2a, 2c, and 2e. Top view of the bottom perturbation profile (h) (scale in meters) is shown in Figures 2b, 2d, and 2f.

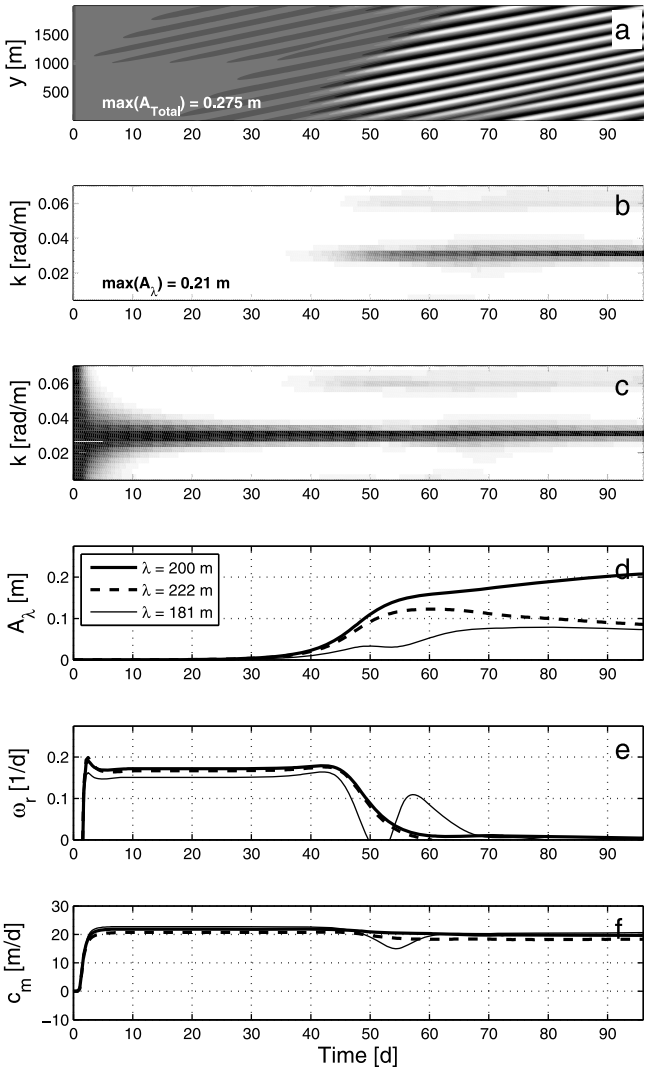

Figure 3. (a) Undisturbed evolution of alongshore bed profile 50 m offshore (white areas crests; black represents troughs). (b) Amplitude development of different lengthscales according to Fourier analysis. (c) Amplitude development normalized at each timestep. (d) Amplitude development for three most dominant lengthscales at each time step. (e) Linear growth rate of these lengthscales. (f) Migration rate.

mode of lengthscale λ. Results for oblique wave incidence are shown; normal wave incidence results are similar. Initial bed pattern development starts in the center of the domain. These bed-forms subsequently spread out and migrate along the shore. In Figures 2c and 2d, small scale crescentic bed-forms can be seen migrating out of the upper end of the modeling domain and re-appearing at the bottom end, due to periodic boundaries. Figures 2e and 2f depicts the stabilized bathymetry, where fully developed crescentic bed-patterns exist over the entire domain. A more detailed description of the bathymetric evolution of one alongshore transect (x = 50 m) is depicted in Figure 3a. It is clearly visible that initial bed pattern formation starts in the center of the modeling domain, which expands and migrates over time. After around 65 days a stable situation has been established and the total amplitude ($A_{Total} = \frac{\max(z_b) - \min(z_b)}{2}$) of fully developed bed-forms along the transect ($\max(A_{\mathrm{Total}})$) is around 30 cm.

[25] Notice that the hydrodynamics are fully coupled with the bed level changes, but no pure hydrodynamic instability is observed. This is, on the face of it, in disagreement with the numerical study by *Yu and Slinn* [2003], which shows, over a similar (but frozen) topography, that rip-currents become unstable (period of oscillations of $\simeq$10–100 min). This discrepancy is mainly attributed to eddy viscosity, which was neglected by *Yu and Slinn* [2003], and which, here, stabilizes the hydrodynamics. *Hasan et al.* [2009], also show that eddy viscosity can damp purely hydrodynamic instabilities in the set-up and circulation, along with the negative feedback provided through increased wave breaking in a non-saturated zone.

[26] In order to investigate the response of the system further, a Fourier analysis is carried out to separate the different crescentic bed pattern lengthscales at different times (see Figure 3b). A_{Total} is composed primarily of the amplitudes of several lengthscales around $k \approx 0.0314$ [rad/m] (λ = 200 m). The amplitude development is normalized at each time step to identify the dominant lengthscales over time (Figure 3c). Initially no dominant lengthscale exists, but after around 40 days several lengthscales develop quickly, and ultimately a dominant lengthscale (λ_{FGM}) of 200 m arises.

[27] To identify the initial response the linear growth is determined, based on the rate of change of the Fourier amplitude (A_λ) (see Figure 3d):

$$\omega_r = \frac{\ln \frac{A_\lambda\,(t=(j+1)\,\Delta t_o)}{A_\lambda\,(t=j\,\Delta t_o)}}{\Delta t_o}, \tag{7}$$

where $A_\lambda\,(t = j\,\Delta t_o)$ is the Fourier amplitude at time $j\,\Delta t_o$, where Δt_o represents the time interval at which the model output is generated (0.35 days). This method enables us to identify the linear growth rate ($\omega_r(\lambda)$) of individual lengthscales. If the growth rate of a lengthscale is constant (and non-zero) for a certain duration, this implies that this Fourier mode is growing (or decaying) linearly. Note that potential cross-shore spatial displacement is interpreted as growth/decay. In all our experiments, the growth during bed pattern development is much larger than the perceived growth/decay caused by cross-shore migration. Thus this formula represents accurately the growth/decay rate of the instability.

[28] The most pronounced lengthscales (λ = 181, 200 and 222 m) all three show linear growth periods (approximately from day 5 to day 45), but λ = 200 m shows a slightly bigger linear growth rate than the other two lengthscales (Figure 3e).

[29] Figure 4 gives growth rates of all lengthscales early in the run (after 5 days), from equation (7). At this time, all bed pattern amplitudes are still negligible, and the development of different lengthscales is unaffected by non-linear interaction. This growth rate curve, therefore, gives a complete overview of the initially developing lengthscales. The initially fastest growing mode (*FGM*) defines the peak of the curve, and also corresponds to the finally dominant mode observed in Figure 3d.

[30] Under oblique wave incidence, crescentic bed patterns migrate alongshore. The Fourier analysis is also used

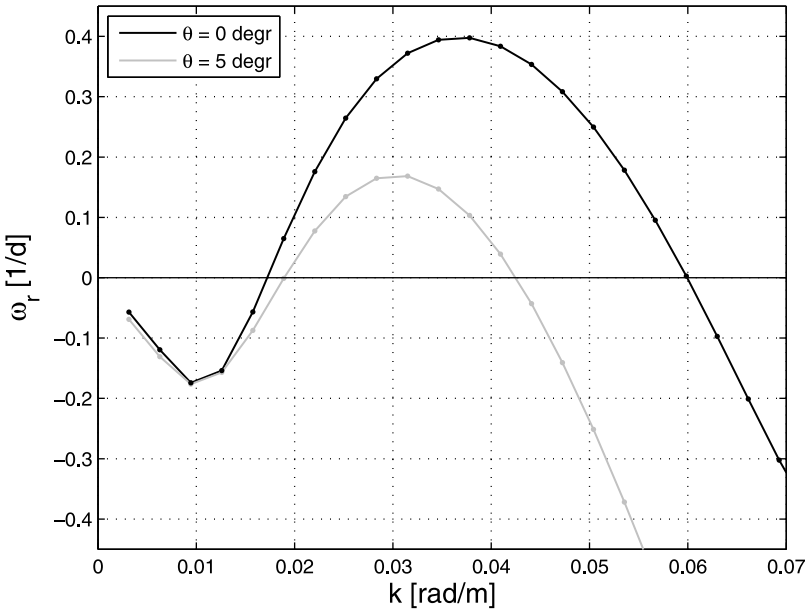

Figure 4. Growth rate curves for both normal (black line) and oblique incidence (grey line) after 5 days. This value remains constant for prolonged periods of time (~10 days) for the fastest growing modes.

to determine the alongshore shift in the bed-form, and so to identify the migration rate (Figure 3f). The full migration rate curve is shown in Figure 5.

4. Evolution in the Presence of Pre-Existing Bed Patterns

4.1. Examples

[31] Three types of evolution can be determined when pre-existing bed patterns are implemented: Breaking up of bed-forms, merging of bed-forms and bed-forms undergoing further growth. An example of the breaking up of pre-existing bed-forms is presented in Figures 6a and 6d, where 666 m long bed-forms are implemented under oblique wave forcing. The dominant lengthscale for undisturbed development (λ_{FGM}) is significantly smaller (200 m) than the initial pre-existing lengthscale ($\lambda_{ini.}$ = 666 m), and the temporal evolution of the alongshore transect shows the breaking up of the pre-existing bed-forms, and the formation of bed patterns with a lengthscale closer to λ_{FGM}. Figure 6a shows how the initial bed-form decreases in amplitude until around day 10, before a new bed-form arises. The decomposition of the overall signal into different frequencies is shown in Figure 6d, along with the undisturbed linear growth rate curve (also shown in Figure 4). Although the pre-existing bed-form breaks up, $\lambda_{final} = 222\ m \neq \lambda_{FGM}$. λ_{final} is in fact a higher harmonic of $\lambda_{ini.}$ ($\lambda_{final} = \frac{\lambda_{ini.}}{3}$), whose undisturbed linear growth rate is closer to that of λ_{FGM}. This behavior is further analyzed in section 4.2.1.

[32] When $\lambda_{ini.} \ll \lambda_{FGM}$ apparently similar behavior to that for $\lambda_{ini.} \gg \lambda_{FGM}$ can be observed (Figures 6c and 6f). Note, however, that the finally dominant bed-form takes longer to develop; that, in this case, $\lambda_{final} = \lambda_{FGM}$ (cf. Figure 6d); and, crucially, note how a continuum of lengthscales develops, centered around λ_{FGM}. In contrast, for $\lambda_{ini.} \gg \lambda_{FGM}$ discrete higher harmonics develop (Figure 6f).

[33] For $\lambda_{ini.}$ closer to λ_{FGM} different behavior can be observed (see Figures 6b and 6e). The pre-existing bed-form remains and does not break up to form shorter bed patterns.

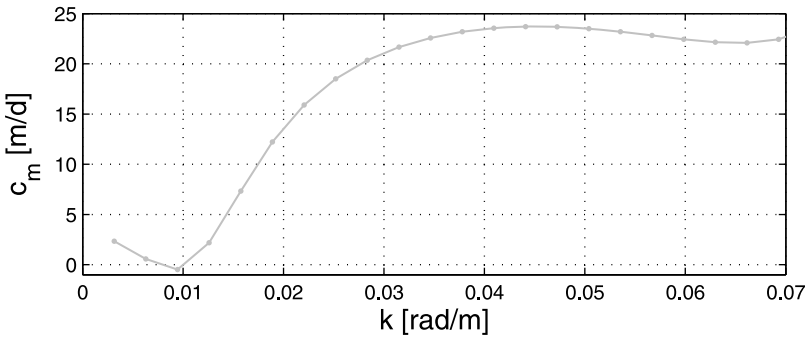

Figure 5. Migration rate curve after 5 days. The migration rate is near-constant over time for the fastest growing modes.

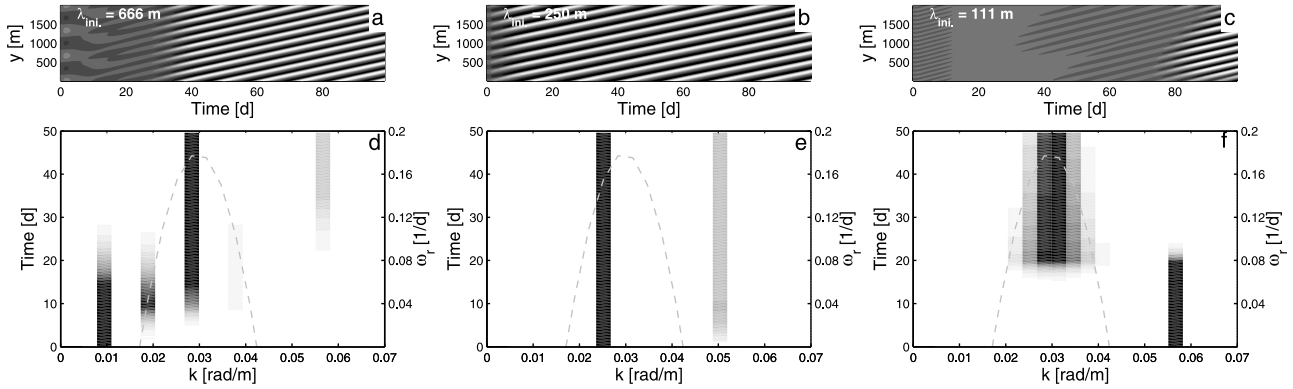

Figure 6. Examples of evolution of nearshore seabed when pre-existing bed patterns are implemented: (a, d) $\lambda_{ini.}$ = 666 m; (b, e) $\lambda_{ini.}$ = 250 m; (e, f) $\lambda_{ini.}$ = 111 m. (a, b, c) Temporal evolution of alongshore transect. Figures 6d, 6e, and 6f show both normalized Fourier analysis, depicting dominance of different length scales in time (black vertical bars, scale on the left), and undisturbed growth rate (grey dashed line, scale on right).

The pre-existing bed-form undergoes further growth, and quickly reaches its maximum amplitude of 0.3 m.

4.2. Lengthscale Evolution

[34] To see the overall picture, results for a wide range of $\lambda_{ini.}$ are presented in Figure 7. The period of dominance of $\lambda_{ini.}$ and λ_{final} can be seen in the left y-axis. The dashed grey curve represents the growth rate curve for the undisturbed development, which is read against the right y-axis. The plotted dominant lengthscales form a slightly schematic description of what is being predicted by the model.

[35] Note that although the pre-existing ($\lambda_{ini.}$) and finally dominant lengthscales (λ_{final}) are correctly represented in Figure 7, the moment when the dominant lengthscale changes is shown here as a direct change over from $\lambda_{ini.}$ to λ_{final}; intermediate stages, which occur, for instance, briefly in Figure 6d, are here omitted for clarity.

[36] Whether imposed bed patterns break up or undergo further growth is closely related to the position of $\lambda_{ini.}$ along the linear growth rate curve. Length scales that show significant linear growth in the undisturbed case remain when implemented as pre-existing bed-forms, while bed-forms that are outside the linear growth rate curve (i.e. they show linear decay in the undisturbed case) disappear when imposed as a pre-existing bed-form. Bed-forms on the edge of the linear growth rate curve show more complex behavior (for example: $k_{ini.}$ = 0.019 [rad/m]) Such lengthscales show initial development, which is subsequently overwhelmed by a bed pattern with a lengthscale that is closer to λ_{FGM}. The results of *Smit* [2010] suggest that pre-existing bed-forms

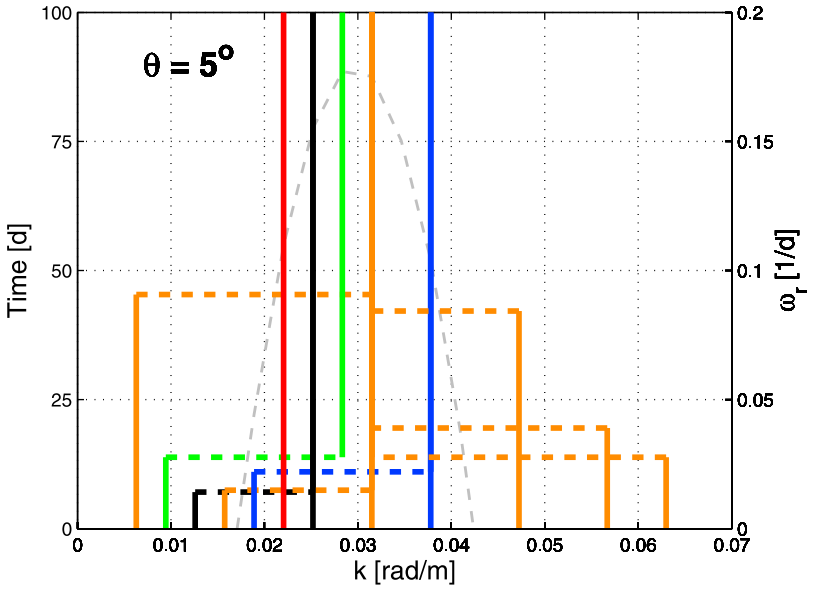

Figure 7. Development of dominant lengthscale for various pre-existing bed pattern lengthscales (solid lines, scale on left), in comparison with growth rate curve for undisturbed development (dashed grey line, scale on right).

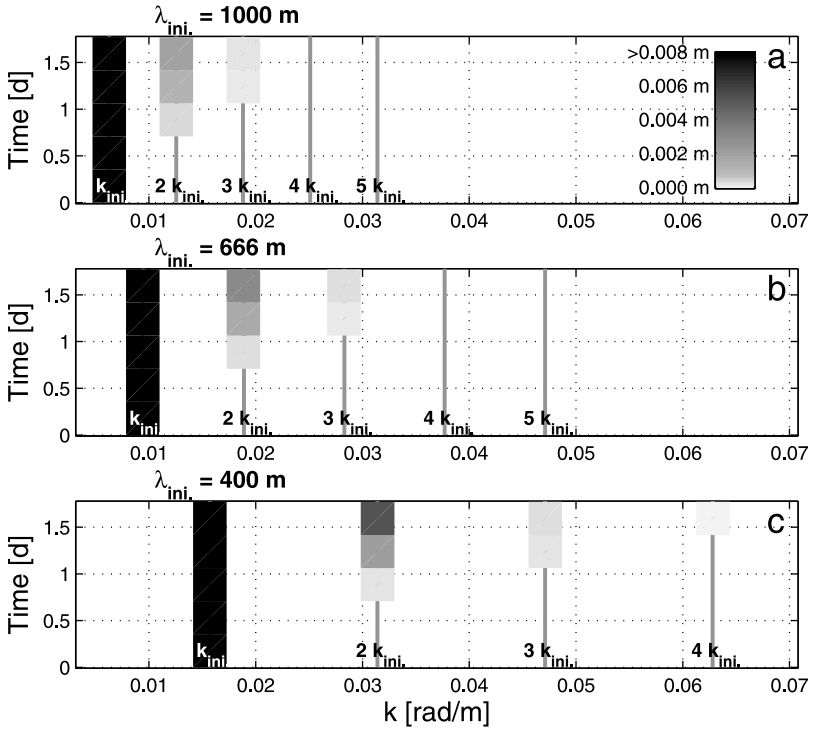

Figure 8. Amplitude development of higher harmonics of $\lambda_{ini.}$ during early stages of model run: (a) $\lambda_{ini.}$ = 1000 m; (b) $\lambda_{ini.}$ = 666 m; (c) $\lambda_{ini.}$ = 400 m. Note that amplitude of $\lambda_{ini.}$ extends beyond range shown in color bar and that for $\lambda_{ini.}$ = 1000 m (Figure 8a), development of λ_{final} ($5k_{ini.}$) occurs later, as a result of interaction between $k_{ini.}$ and $4k_{ini.}$.

are only transformed into bed patterns with a different lengthscale if the pre-existing bed-forms develop over a short duration, and only possess limited amplitudes. In each case, however, they determine one single weighted-average dominant lengthscale at each moment, which obscures any possible link between the undisturbed linear growth rate curve and the development of pre-existing bed patterns.

4.2.1. Initial Development of Higher Harmonics of $\lambda_{ini.}$

[37] For a pre-existing lengthscale to persist, its undisturbed (linear) growth rate is critical. However, if bed-forms break up or merge, λ_{final} is not always λ_{FGM}. For $\lambda_{ini.} \gg \lambda_{FGM}$, $\lambda_{ini.}$ ultimately gives rise to one of its harmonics (Figure 8). Thus, e.g., $\lambda_{ini.}$ = 1000 m, under both normal and oblique wave incidence, splits into λ_{final} = 200 m, which shows considerable linear growth in the undisturbed case and is close to λ_{FGM} (Table 2). The initial bed-form generates higher harmonics via self-interaction, so that longer pre-existing wavelengths generate short lengthscales closer to λ_{FGM} [see, e.g., *Schielen et al.*, 1993]. Initially, it is mainly the second and third harmonics ($\frac{\lambda_{ini.}}{2}$ and $\frac{\lambda_{ini.}}{3}$) that increase in amplitude. This effect can be seen in Figure 6d: Initially $\lambda_{ini.}$ (666 m) is dominant, however, after approximately 10 days, the dominant lengthscale briefly becomes $\frac{\lambda_{ini.}}{2}$ (333 m) before switching to $\frac{\lambda_{ini.}}{3}$ (222 m), which remains dominant until the end of the modeling run. $\frac{\lambda_{ini.}}{3}$ possesses a significantly larger undisturbed linear growth rate than $\frac{\lambda_{ini.}}{2}$ or $\lambda_{ini.}$.

[38] For $\lambda_{ini.}$ = 666 m for θ = 0 (not shown) the undisturbed linear growth rate of $\frac{\lambda_{ini.}}{4}$ (166 m, k = 0.038 [rad/m]) is bigger than that of $\frac{\lambda_{ini.}}{3}$ (222 m). However, this higher harmonic only shows very limited amplitude development by non-linear interaction. As a result, subsequent development of $\frac{\lambda_{ini.}}{4}$ does not overtake $\frac{\lambda_{ini.}}{3}$ and $A_{\lambda_{ini.}/4}$ remains smaller than $A_{\lambda_{ini.}/3}$.

[39] If $\lambda_{ini.} \ll \lambda_{FGM}$, the decay in height of the imposed bed-forms occurs for a prolonged period, before new bed-forms arise (see Figure 6f). λ_{final} is, in this case, not a factor of $\lambda_{ini.}$, but generally equal to λ_{FGM}. Higher harmonics are generated, but these even shorter lengthscales are further outside the linear growth rate curve and decay (even more rapidly) along with the pre-existing bed patterns. The pre-existing bed-form, therefore, only loses dominance when background noise creates bed-forms with a lengthscale that shows linear growth, in general favoring λ_{FGM}.

Table 2. Initial and Finally Dominant Lengthscales for Normal and Oblique Wave Incidence, and Factor (c_h) by Which the Number of Bed-Forms Along a Certain Beach Width Increases

		θ = 0°		θ = 5°	
$\lambda_{ini.}$ [m]	$k_{ini.}$ [rad/m]	λ_{final} [m]	c_h [-]	λ_{final} [m]	c_h [-]
1000	0.0063	200	5	200	5
666	0.0094	222	3	222	3
500	0.0126	166	3	250	2
400	0.0157	200	2	200	2
333	0.0189	166	2	166	2
286	0.0220	286	–	286	–
250	0.0251	250	–	250	–
200	0.0314	200	–	200	–
166	0.0379	166	–	166	–
133	0.0472	133	–	200	0.67
111	0.0566	200	0.56	200	0.56
100	0.0628	166	0.60	200	0.50

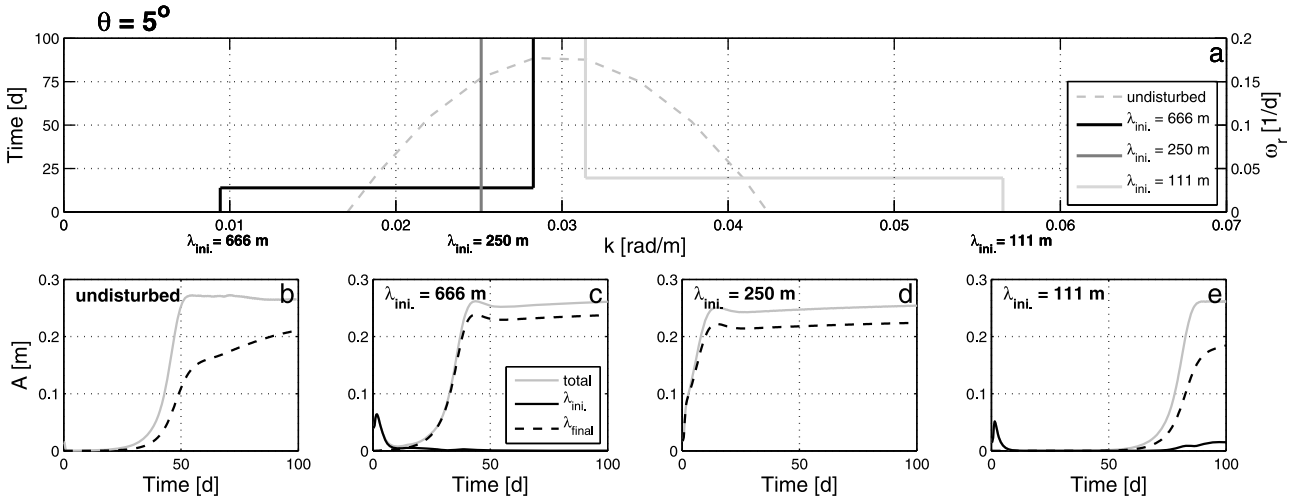

Figure 9. Bed pattern development for different $\lambda_{ini.}$ in comparison with undisturbed bed pattern development. (a) Overview of bed pattern lengthscale development of different pre-existing lengthscales (grey scale, scale on left), along with undisturbed linear growth rate curve determined after 5 days of development (dashed, scale on right). Amplitude development of A_{Total} as well as $A_{\lambda_{ini.}}$ and $A_{\lambda_{final}}$ of the alongshore transect; (b) undisturbed beach (λ_{FGM} = 200 m) ($\lambda_{ini.}$ does not exist), (c) long pre-existing bed-patterns ($\lambda_{ini.}$ = 666 m), (d) pre-existing bed patterns with lengthscale close to λ_{FGM} ($\lambda_{ini.}$ = 250 m), and (e) short pre-existing bed patterns ($\lambda_{ini.}$ = 111 m).

4.2.2. General Observations

[40] A clear relationship between $\lambda_{ini.}$ and the time when the dominant lengthscale changes is not directly apparent, and depends on both the growth of λ_{final} and the decay of $\lambda_{ini.}$.

[41] For $\lambda_{ini.} \gg \lambda_{FGM}$, the duration before a bed-form breaks up generally decreases with decreasing $\lambda_{ini.}$ (see Figure 7).

[42] The reason for this appears to be increased steepness of bed-forms: shorter pre-existing bed-forms are steeper morphological features for the same amplitude; this results in increased development of higher harmonics: see Figures 8a, 8b, and 8c. $\lambda_{ini.}$ = 333 m (k = 0.018 [rad/m]) is inconsistent with this (see Figure 7), but it should be recalled that this lengthscale is on the edge of the linear growth rate curve, and shows initial growth itself before being overtaken by a faster growing higher harmonic of $\lambda_{ini.}$.

[43] For $\lambda_{ini.} \ll \lambda_{FGM}$ a similar relationship can be observed, but the duration before the lengthscale changes is much longer. The more rapid change from $\lambda_{ini.}$ to λ_{final} for smaller $\lambda_{ini.}$ appears to be the result of the increased decay rate of the shorter pre-existing lengthscales; since λ_{final} is not a higher harmonic of (i.e. not directly excited by) $\lambda_{ini.}$, its development is similar for different $\lambda_{ini.}$.

4.3. Amplitude Evolution

[44] The evolution of the amplitude of the bed patterns can give information concerning the speed at which bed-forms reach their final height and the time at which the dominant lengthscale changes. The amplitude evolution is closely linked to $\lambda_{ini.}$ (Figure 9). If $\lambda_{ini.} \approx \lambda_{FGM}$ the development of the bathymetry to a final state is accelerated (Figure 9d), compared to the undisturbed case (Figure 9b). The cases for which $\lambda_{ini.} \lesssim \lambda_{FGM}$ show differing longer durations before the final height is reached (Figures 9c and 9e). The duration before the final height is reached is considerably longer for $\lambda_{ini.} \ll \lambda_{FGM}$ than for $\lambda_{ini.} \gg \lambda_{FGM}$; presumably in the latter case the initial development of λ_{final} is accelerated due to higher harmonic interactions (see previous section).

[45] To investigate the importance of the initial amplitude, $A_{ini.}$ is varied for one $\lambda_{ini.} \gg \lambda_{FGM}$ ($\lambda_{ini.}$ = 500 m, θ = 5°): see Figure 10. The development of $A_{\lambda_{ini.}}$ and $A_{\lambda_{final}}$ capture the decay of the pre-existing mode, and the subsequent development of the finally dominant one. The development time ($t_{0.95A_{Total}(t_{final})}$) is defined as the time when A_{Total} first achieves 95% of its final value ($A_{Total}(t_{final})$), which gives a good representation of when the bed achieves a stable finite amplitude. The time ($t_{min(A_{Total})}$) when A_{Total} is at a minimum roughly corresponds to the moment at which the dominant lengthscale changes from $\lambda_{ini.}$ to λ_{final}. The time (about 1.8 days) at which the pre-existing bed-form achieves its maximum amplitude (due to the shoreward shift of the bed-forms, during the start-up of the model runs) is, in essence, an adjustment period during which generation of higher harmonics does occur, but in which linear behavior is not apparent. The amplitude of the finally dominant lengthscale at this time ($min(A_{\lambda_{final}})$) therefore gives an indication of the rate of higher harmonic interaction. Note that the amplitudes shown are those at the 50 m transect, so that $A_{\lambda_{ini.}}(t = 0) \leqslant A_{ini.}$, the latter value referring to the maximum amplitude of the pre-existing mode over the whole domain.

[46] Increasing values of $A_{ini.}$ result in a more rapid development of λ_{final} and the quicker stabilization of the bed (Figure 10a), and $t_{min(A_{Total})}$ and $t_{0.95A_{Total}(t_{final})}$ both decrease for increasing $A_{ini.}$ (Figure 10b). This is consistent with a larger initial amplitude leading to more non-linearity and stronger self-interaction of the pre-existing mode, so that more energy is fed into $A_{\lambda_{final}}$ (note the faster-than-linear increase of $min(A_{\lambda_{final}})$ with respect to $A_{ini.}$: Figure 10e). The increase in $min(A_{Total})$ (Figure 10c) is also consistent with this, since at this moment A_{Total} is roughly composed of both $A_{\lambda_{ini.}}$ and $A_{\lambda_{final}}$, which increase for bigger $A_{ini.}$. Note too that in the absence of harmonic generation an increase in $A_{ini.}$

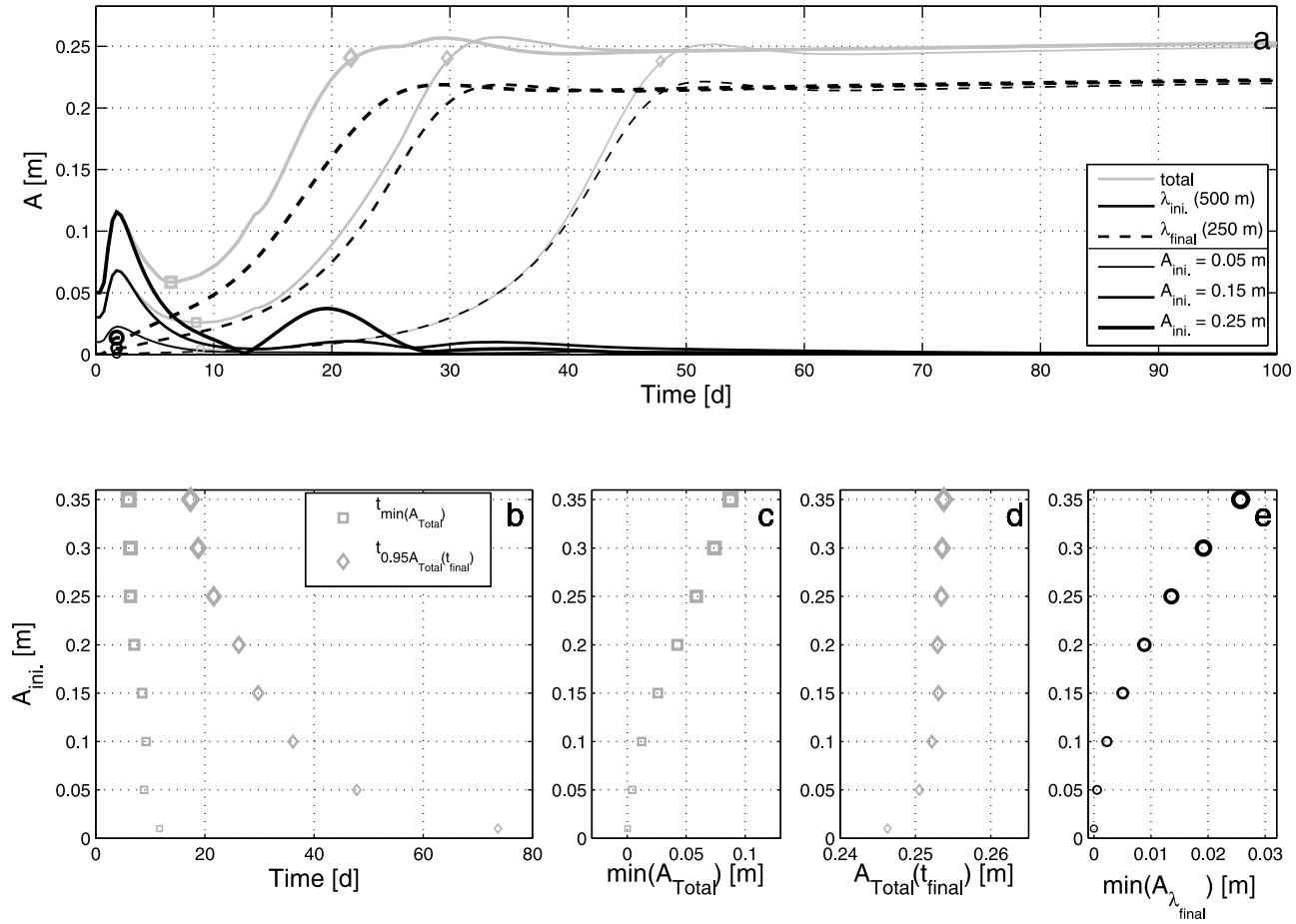

Figure 10. Influence of different $A_{\text{ini.}}$ on the subsequent crescentic bed pattern evolution ($\lambda_{\text{ini.}} = 500$ m). (a) The development of A_{Total} (grey line), $A_{\lambda_{\text{ini.}}}$ (solid black line), and $A_{\lambda_{\text{final}}}$ (dashed black line) for different $A_{\text{ini.}}$ (line thickness). The effect of varying $A_{\text{ini.}}$ on: (b) $t_{\min(A_{\text{Total}})}$ (square) and $t_{0.95A_{\text{Total}}(t_{\text{final}})}$ (diamond); (c) $\min(A_{\text{Total}})$ (square); (d) $A_{\text{Total}}(t_{\text{final}})$ (diamond); (e) $\min(A_{\lambda_{\text{final}}})$ (circle).

might be thought to lead to a longer period of dominance of $\lambda_{\text{ini.}}$, as this mode would then decay for longer. The opposite happens, however, indicating the presence of finite amplitude effects, and the faster rise to dominance of $A_{\lambda_{\text{final}}}$. $A_{\text{Total}}(t_{\text{final}})$ is reasonably constant for various $A_{\text{ini.}}$ (Figure 10d), suggesting that the pre-existing amplitude does not affect the final bed pattern height. Note that regardless of $A_{\text{ini.}}$ a small but significant proportion of A_{Total} remains in modes other than λ_{final} even during the latter stages of crescentic bed-pattern evolution; this is especially so for oblique wave incidence. These lengthscales are generally higher harmonics of λ_{final} (as can be seen in Figures 6d and 6e) and lead to asymmetry of the bed-forms.

[47] A more detailed analysis of the impact of different $A_{\text{ini.}}$ and $\lambda_{\text{ini.}}$ on subsequent development of various characteristic measures ($t_{\min(A_{\text{Total}})}$, $t_{0.95A_{\text{Total}}(t_{\text{final}})}$, $\min(A_{\text{Total}})$ and $\min(A_{\lambda_{\text{final}}})$) is shown in Figures 11 and 12 and discussed hereafter.

4.3.1. $\lambda_{\text{ini.}} \gg \lambda_{\text{FGM}}$

[48] The combined effect that i) increasing $k_{\text{ini.}}$ yield more non-linear pre-existing bed-forms and so more energy is fed into higher harmonics, and ii) that for increasing $k_{\text{ini.}}$ lower order higher harmonics will result in significant linear growth (in the undisturbed scenario), both result in the more rapid establishment of λ_{final}, for increased $k_{\text{ini.}}$ (reduced $t_{\min(A_{\text{Total}})}$, Figure 11a), and a more rapid development to a new stable situation (reduced $t_{0.95A_{\text{Total}}(t_{\text{final}})}$, Figure 11b). The increased energy being fed into higher harmonics, for increased $k_{\text{ini.}}$, can be seen in the increased $\min(A_{\lambda_{\text{final}}})$ (Figure 12c), and, as a result, there is a more limited decline of A_{Total} before the development of λ_{final} takes over (increasing $\min(A_{\text{Total}})$, Figure 12a).

[49] The effect on $t_{\min(A_{\text{Total}})}$ of increasing $A_{\text{ini.}}$ is significantly less than that of increasing $k_{\text{ini.}}$, due to two opposite effects: More energy is fed into λ_{final} (see Figure 12c), but also the decay of $\lambda_{\text{ini.}}$ is prolonged for increased $A_{\text{ini.}}$. As a result, $t_{0.95A_{\text{Total}}(t_{\text{final}})}$ decreases and $\min(A_{\text{Total}})$ increases for increased $A_{\text{ini.}}$ (Figures 11b and 12a). The effect of $A_{\text{ini.}}$ on $t_{\min(A_{\text{Total}})}$ is notably stronger as $k_{\text{ini.}} \rightarrow 0$. This is probably because the dependence of $t_{0.95A_{\text{Total}}(t_{\text{final}})}$ on $A_{\text{ini.}}$ becomes increasingly non-linear as more harmonics are involved in the process of shifting energy from $k_{\text{ini.}}$ to k_{final}.

4.3.2. $\lambda_{\text{ini.}} \ll \lambda_{\text{FGM}}$

[50] As also discussed earlier, in these circumstances higher harmonic development does not cause lengthscales close to λ_{FGM} to arise. The development of λ_{final} originates only from background noise. The result is a significantly slower development of λ_{final} (Figure 11b).

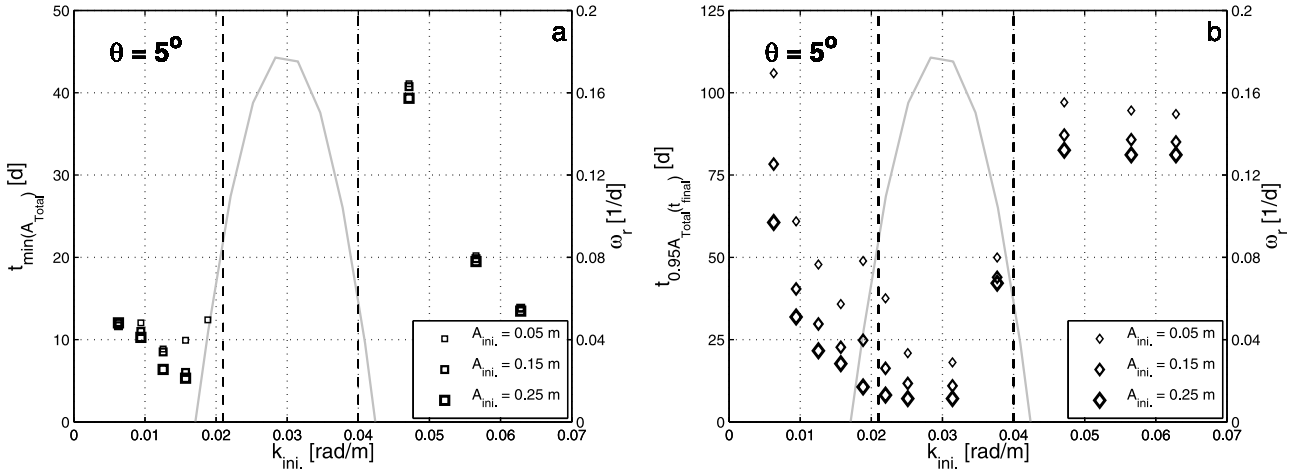

Figure 11. (a) $t_{\min(A_{\text{Total}})}$ (scale on left) and (b) $t_{0.95A_{\text{Total}}(t_{\text{final}})}$ (scale on left) for various initial lengthscales and amplitudes (marker size). The grey line represents the undisturbed linear growth rate curve (scale on right). Dashed vertical lines represent the range within which initial lengthscales do not break up or merge, but undergo further growth.

[51] Also note the very small values of $\min(A_{\text{Total}})$ and $\min(A_{\lambda_{\text{final}}})$ for $k_{\text{ini.}} \gg k_{\text{FGM}}$ compared to those for $k_{\text{ini.}} \ll k_{\text{FGM}}$.

[52] Variation in the initial lengthscale has a more complex influence on the subsequent bathymetric evolution than for $\lambda_{\text{ini.}} \gg \lambda_{\text{FGM}}$. Increased $k_{\text{ini.}}$ causes a very limited increase of background noise, seemingly due to increased steepness of pre-existing modes, and λ_{final} is among the lengthscales that profit from this effect (see Figure 12d). This results in minor changes to $t_{0.95A_{\text{Total}}(t_{\text{final}})}$ (most visible for small $A_{\text{ini.}}$ in Figure 11b). However, for increased $k_{\text{ini.}}$ modes also have an increased decay rate (see Figure 4), which causes the decline of $\lambda_{\text{ini.}}$ modes to be accelerated, and results in more rapid dominance of λ_{final} (Figure 11a, although this can also to a limited degree be attributed to increased background noise). The increased decay rate of $\lambda_{\text{ini.}}$ (as $k_{\text{ini.}}$ increases) has a much stronger influence than the increased background noise; $\min(A_{\text{Total}})$ significantly decreases for bigger $k_{\text{ini.}}$ (see Figure 12b).

[53] Note that the influence of the rate of decay of $\lambda_{\text{ini.}}$, as discussed for $\lambda_{\text{ini.}} \ll \lambda_{\text{FGM}}$, also applies for $\lambda_{\text{ini.}} \gg \lambda_{\text{FGM}}$. However, the rate of decay is significantly more rapid for $\lambda_{\text{ini.}} \ll \lambda_{\text{FGM}}$, and the effect of increased higher harmonic interaction for $\lambda_{\text{ini.}} \gg \lambda_{\text{FGM}}$ (for increased $k_{\text{ini.}}$) obscures any influence that might be the result of the variations in decay rate.

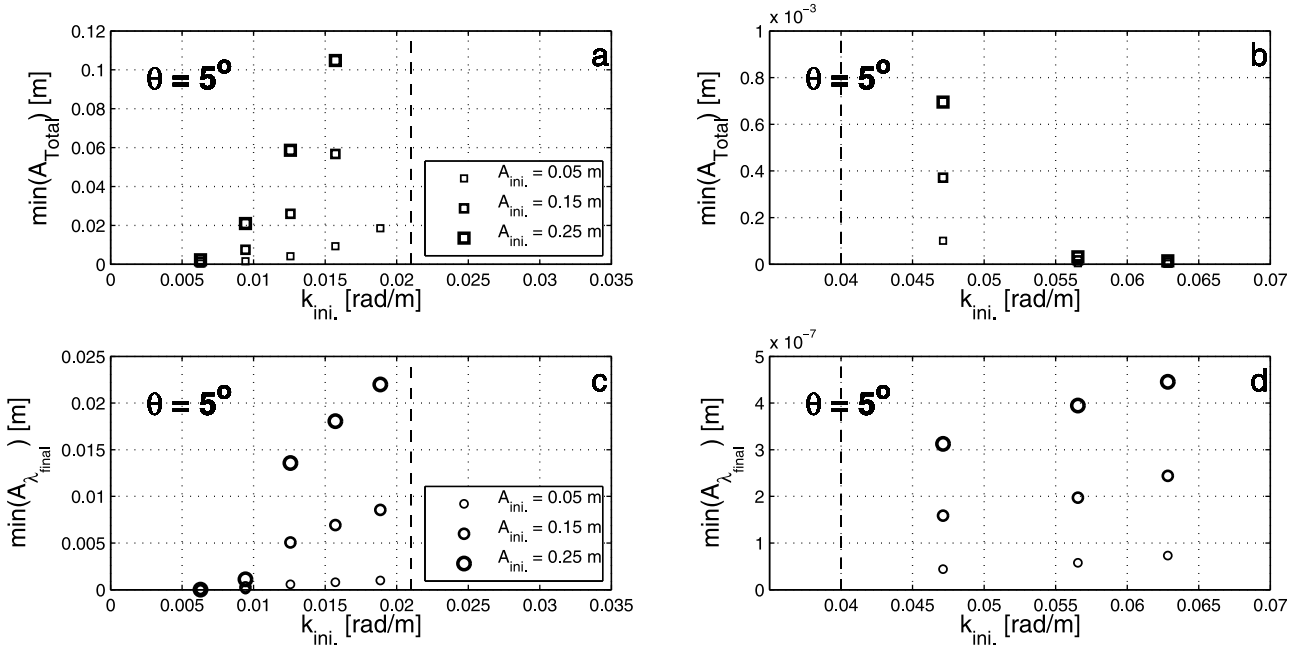

Figure 12. (a, b) $\min(A_{\text{Total}})$ and (c, d) $\min(A_{\lambda_{\text{final}}})$ for different initial lengthscales and amplitudes (marker size). The amplitudes for $k_{\text{ini.}} < 0.035$ [rad/m] are plotted in a separate graph, since these are significantly bigger than those of $k_{\text{ini.}} > 0.035$ [rad/m].

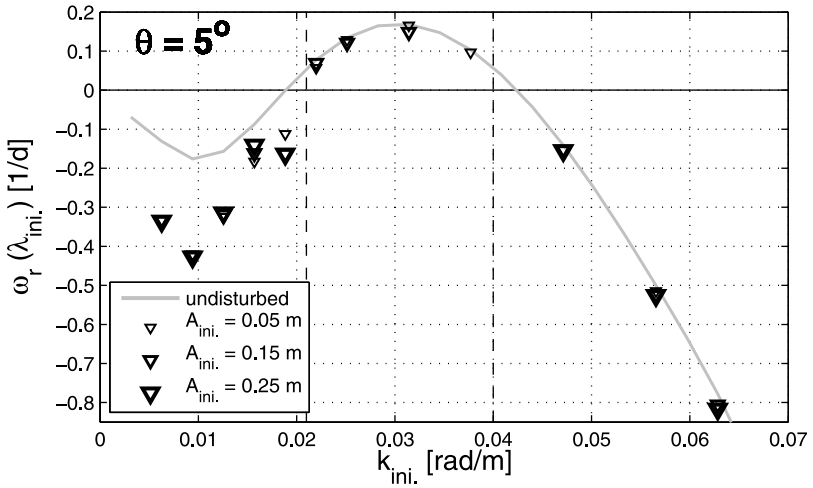

Figure 13. Linear growth and decay rates for various $\lambda_{ini.}$ and $A_{ini.}$ (marker size). These results are compared with undisturbed linear growth after five days of development (grey line). Dashed lines show range of lengthscales that remain and do not break up or merge.

[54] Variation of $A_{ini.}$ appears to have much the same effect as for $\lambda_{ini.} \gg \lambda_{FGM}$, although significantly smaller in absolute values; increased $A_{ini.}$ cause the newly arising bed-form initially to develop more quickly ($\min(A_{\lambda_{final}})$, Figure 12d) and reach a new stable situation earlier (Figure 11b). The influence of $A_{ini.}$ on $t_{\min(A_{Total})}$ and $\min(A_{Total})$ is limited and generally overwhelmed by the influence of $k_{ini.}$ (Figures 11a and 12b).

4.3.3. $\lambda_{ini.} \approx \lambda_{final}$ and Marginal Modes

[55] Values of $k_{ini.}$ that possess the biggest growth rates, reach a final height earlier than $k_{ini.}$ that are closer to the edge of the growth rate curve (as can especially be seen for small $A_{ini.}$ in Figure 11b). Increased values of $A_{ini.}$ also result in a smaller $t_{0.95A_{Total}(t_{final})}$.

[56] Note that $\min(A_{Total})$ and $t_{\min(A_{Total})}$ do not exist for these $\lambda_{ini.}$, because these lengthscales only increase in amplitude. Since $\lambda_{ini.} = \lambda_{final}$, the value of $\min(A_{\lambda_{final}})$ is the result of $A_{ini.}$, and of no use for the analysis of subsequent bathymetric evolution.

[57] As described in section 4.2, $\lambda_{ini.}$ that are at the edge of the linear growth rate curve persist and show initial development, before being overwhelmed by faster growing lengthscales closer to λ_{FGM}. In these cases $\min(A_{Total})$ and $t_{\min(A_{Total})}$ do not generally exist either, since A_{Total} is monotonically increasing (in Figures 11a and 12a) for $k_{ini.} = 0.019$ [rad/m], $A_{ini.} = 0.05$ m is shown, but for larger values of $A_{ini.}$ a minimum amplitude cannot be identified).

4.3.4. General Observations

[58] As was already observed for one pre-existing length scale (Figure 10), $A_{Total}(t_{final})$ is near-constant for different values of $A_{ini.}$. $A_{Total}(t_{final})$-values for all bed-forms are also independent of $\lambda_{ini.}$, but depend on λ_{final} (not shown).

[59] Secondly, $A_{ini.}$ does not cause differences in λ_{final} (not shown). This is a main difference from the results presented by *Smit* [2010], who observe some dependence of the average lengthscale on the amplitude of the pre-existing bed-forms. *Coco et al.* [2000] investigate the development of beach cusps in a similar way as presented here; their findings (although for a very different bed pattern) suggest that bed patterns of any amplitude break up if the pre-existing lengthscale is more than a factor of two different from the lengthscale that would develop from an undisturbed beach. An increased amplitude of the pre-existing bed patterns only causes a widening of the range of lengthscale that persist. This corresponds, to an extent, with the results obtained here, because lengthscales that are on the edge of the linear growth rate curve (i.e. near to zero linear growth) show significantly different behavior from those further inside or outside the curve. Increased initial amplitudes of these lengthscales can result in prolonged periods of dominance of $\lambda_{ini.}$, and even remains dominant throughout the modeling period (not shown). In this case, pre-existing bed-forms with large amplitudes generate a strong rhythmic current, which is comparable in intensity to the current obtained in the undisturbed case. This solid coupling between the pre-existing morphology and hydrodynamics is difficult to break under these conditions.

[60] For wider growth rate curves (for instance, for smaller γ, see section 6.1), this range of boundary-growth lengthscales could be of bigger importance, especially if multiple pre-existing lengthscales were to co-exist (see section 4.6).

4.4. Linear Growth Rate

[61] The linear growth rate (ω_r) gives information about the initial evolution of bed-forms. In fully non-linear development, linear growth can only be expected to occur initially, when amplitudes are small. If in the case of pre-existing, finite-amplitude bed patterns, the finally dominant bed-forms display periods of linear growth then we may assume that linear stability analyses correctly describe morphological evolution, at least in part, as a beach evolves from one complex state to another. We turn to this next (Figures 13 and 14).

[62] The presence of different $\lambda_{ini.}$ leads to different amplitude development (see Figure 14a), due to growth or decay of the pre-existing mode and the rise of the finally dominant mode (Figures 14d, 14g, and 14i).

[63] For cases when the $\lambda_{ini.}$ mode disappears, clear linear growth of λ_{final} is apparent (Figures 14e and 14j), i.e. a

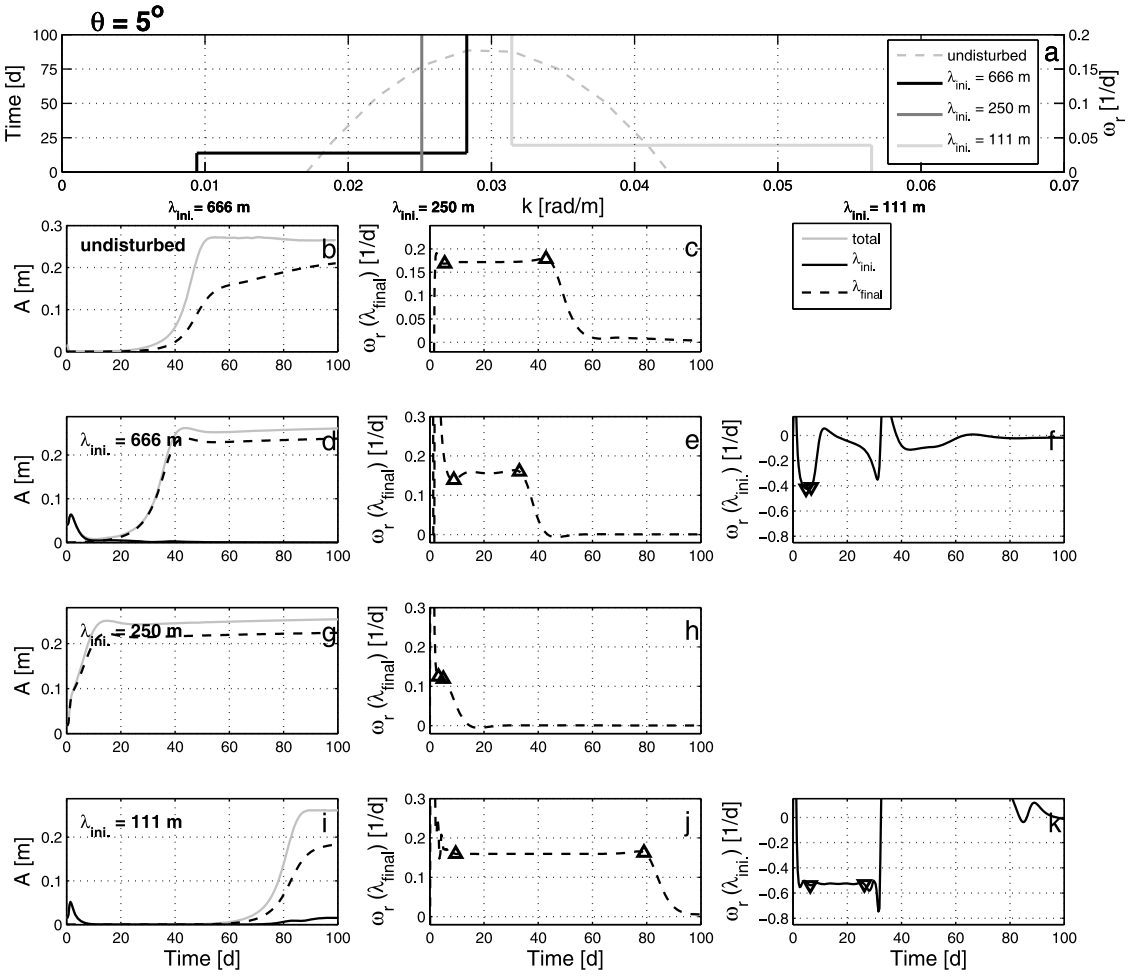

Figure 14. Occurrence of linear growth periods for different pre-existing bed pattern lengthscales, in comparison with bed pattern development starting from alongshore constant beach profile. Results are presented in a similar way as in Figure 9; (a) Overview of bed pattern lengthscale development of different pre-existing lengthscales. (b, d, g, i) Development of A_{Total} as well as $A_{\lambda_{\mathrm{ini.}}}$ and $A_{\lambda_{\mathrm{final}}}$ for undisturbed development and for different pre-existing bed patterns. (c, e, h, j) ω_r from equation (7) of λ_{final}, periods of constant growth are marked with the triangle. If pre-existing bed pattern breaks up: (f, k) ω_r of $\lambda_{\mathrm{ini.}}$, where periods of constant decay are marked with the inverted triangle.

duration with quasi-constant ω_r (λ_{final}); this linear growth period is comparable to that in the undisturbed scenario (Figure 14c). Note that for $\lambda_{\mathrm{ini.}} = 111$ m the linear growth period (between the triangular markers) exceeds that for the undisturbed scenario, apparently because the 'Dirac' perturbation (of 0.03 m) excites more energy at λ_{final} than does the pre-existing lengthscale ($A_{\mathrm{ini.}} = 0.15$ m). Of particular interest is the linear growth period for $\lambda_{\mathrm{ini.}} = 666$ m, which is shorter than for the undisturbed scenario, despite ω_r being essentially identical. Evidently, energy is fed into λ_{final} via harmonic interaction ($k_{\mathrm{ini.}} \rightarrow 2k_{\mathrm{ini.}} \rightarrow k_{\mathrm{ini.}} + 2k_{\mathrm{ini.}}$). Nonetheless λ_{final} does grow freely (hence the linear growth—note that the initial "adjustment period" prior to constant linear growth is larger for Figure 14e, than for Figures 14c and 14j). In contrast, a period of constant linear growth is almost nonexistent for the bed-form that persists (Figure 14h), due to the increased initial amplitude, and therefore non-linearity. In Figures 14c, 14e, and 14j, the linear growth period continues until the newly arising bed-pattern reaches a threshold amplitude, and non-linear effects become significant. The growth (decay) rate is also presented for decaying pre-existing bed patterns (Figures 14f and 14k). $\lambda_{\mathrm{ini.}} = 111$ m clearly decays linearly from day 3 to day 28. For $\lambda_{\mathrm{ini.}} = 666$ m there is a possibly linear decay from day 3 to day 5, but apart from that there is no such behavior, which is consistent with energy being fed into higher harmonics.

[64] Linear growth and decay are defined as a change in growth rate of less than 2% between two consecutive measurements, persisting for at least four time steps ($\Delta t_o = 0.35$ d). Periods that satisfy these conditions can be found both during the growth of λ_{final} (marked with an open triangle) as well as (more briefly) during the decay periods of $\lambda_{\mathrm{ini.}}$ (marked with an inverted triangle) in Figure 14.

[65] The periods of linear growth and decay vary for different $A_{\mathrm{ini.}}$ (not shown). The period of constant linear growth of λ_{final} reduces for increasing $A_{\mathrm{ini.}}$ as expected. A greater $A_{\mathrm{ini.}}$ leads to more energy being fed to λ_{final} (therefore increased amplitude and reduced linear growth period). Increased $A_{\mathrm{ini.}}$ also results in prolonged periods of constant linear decay for $\lambda_{\mathrm{ini.}}$. However, for very large values of $A_{\mathrm{ini.}}$,

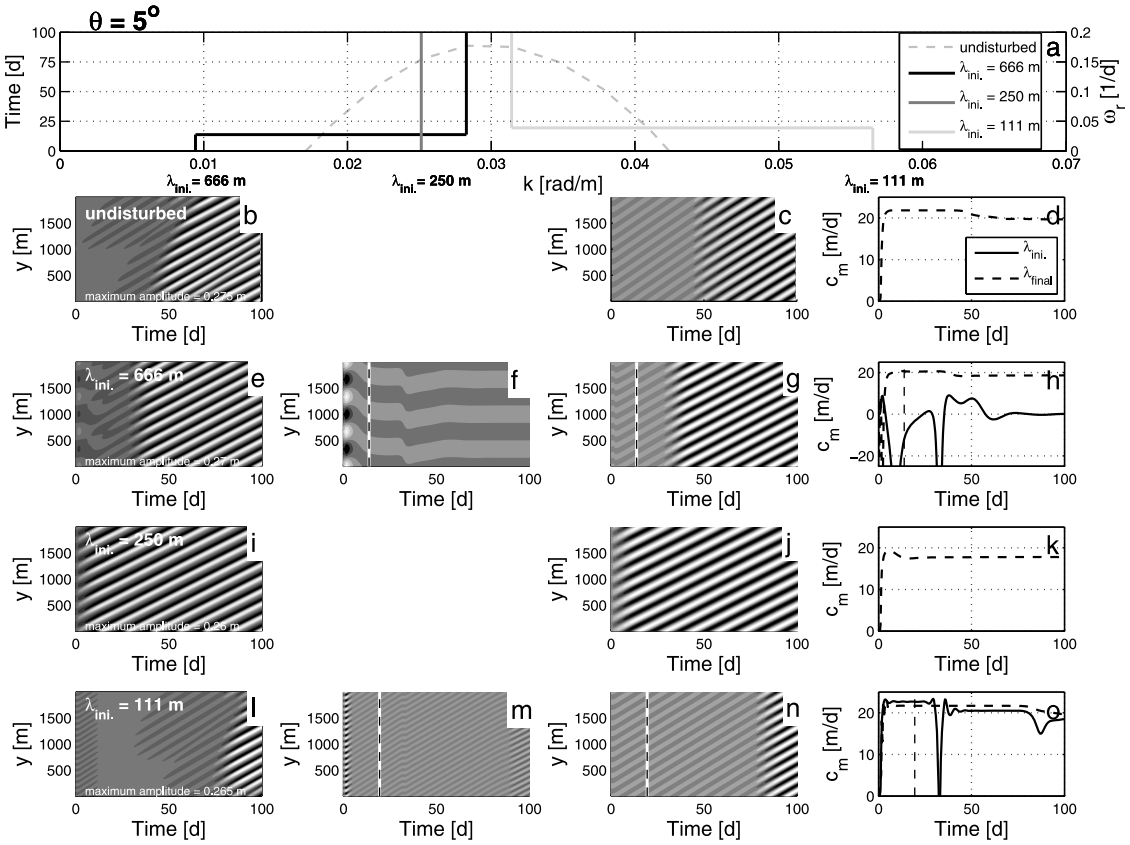

Figure 15. Migration for different $\lambda_{ini.}$ in comparison with undisturbed bed pattern development. Results are presented in a similar way as in Figure 9: (a) Overview of bed pattern lengthscale development of different pre-existing lengthscales. (b, e, i, l) Total bed pattern development along the alongshore transect (crests white, troughs black). Total bed pattern development decomposed into bed pattern development for different lengthscales: (f, m) $\lambda_{ini.}$ and (c, g, j, n) λ_{final}. (d, h, k, o) Migration rates for $\lambda_{ini.}$ and λ_{final} from decomposed bed pattern evolution. Dashed line (Figures 15f, 15g, 15m, and 15n) represents the moment when the dominance switches from $\lambda_{ini.}$ to λ_{final}.

this relationship becomes less clear, partially due to increased non-linear effects and because of the more rapid development (and dominance) of λ_{final}. The growth and decay rates during the linear growth periods are quasi-constant for all $A_{ini.}$ (not shown).

[66] For different values of $\lambda_{ini.}$ (Figure 13), a close correspondence between the computed ω_r of the pre-existing bed-forms and the undisturbed growth rate curve can be observed. Differences mainly occur for decaying bed-forms with big lengthscales ($k_{ini.} < 0.02$ [rad/m]), where the decay rate of the pre-existing bed-forms is larger than that observed for undisturbed development.

[67] Lengthscales that are on the boundary between decay and growth (for example: $\lambda_{ini.} = 333$ m ($k_{ini.} = 0.019$ [rad/m]), $A_{ini.} = 0.15$ m) are generally absent from Figure 13. As described in section 4.3, these lengthscales show limited linear growth in the undisturbed scenario and, when implemented as pre-existing bed-forms, are overwhelmed by faster developing lengthscales that occur in the center of the growth rate curve. These initial lengthscales generally exhibit only a very gradual increase or decrease in amplitude, and limited or no constant linear growth.

[68] This qualitatively different behavior of these marginal initial lengthscales also occurs for $\omega_r(\lambda_{final})$ (not shown). Growth rates of the finally dominant lengthscales generally correspond well with those of the undisturbed case, regardless of $A_{ini.}$, except for marginal modes. As $A_{ini.}$ increases for these modes, $\omega_r(\lambda_{final})$ diverges from that given in the undisturbed case, apparently because two distinct modes are evolving; the $\lambda_{ini.}$-mode of finite amplitude is interfering with the linear development of the λ_{final}-mode.

4.5. Migration Rate

[69] Previous research using a non-linear stability analysis has generally studied the development of crescentic bed patterns from an 'infinitesimal' perturbed alongshore constant beach [e.g., *Garnier et al.*, 2006; *Klein*, 2006; *Smit et al.*, 2008]. Migration rates have been relatively easy to obtain, since one lengthscale would generally dominate the development [*Garnier*, 2006]. In the present study, the migration rate of both the initial lengthscale ($c_m(\lambda_{ini.})$) and the finally dominant lengthscale ($c_m(\lambda_{final})$) are determined (Figure 15) and compared with that of the undisturbed case (Figure 15b). For the different λ_{final}, $c_m(\lambda_{final})$ is quasi-constant in time, ≈20 m/d (Figures 15h, 15k, and 15o) (with a slightly smaller migration rate for $\lambda_{ini.} = 250$ m). $c_m(\lambda_{ini.})$ are more variable over time. The pre-existing bed-patterns (obtained from the Morfo60 linear stability model) are for

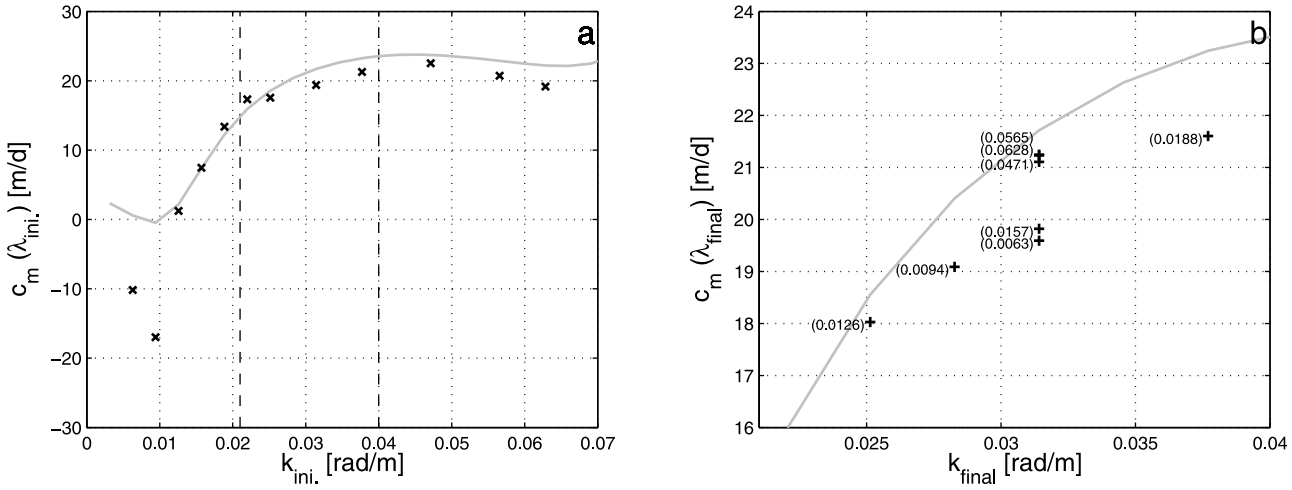

Figure 16. Migration rate of (a) $\lambda_{ini.}$ and (b) λ_{final} for different $\lambda_{ini.}$ ($A_{ini.}$ = 0.15 m). Average migration rate is plotted over period for which $\lambda_{ini.}$ and λ_{final} are dominant. Undisturbed migration rate (at day 5) plotted as a grey line. Dashed lines show the range within which lengthscales remain, and do not break up or merge. Values between brackets represent k-value of the different examined pre-existing lengthscales (see Table 2 for the corresponding $\lambda_{ini.}$-values).

normally incident waves and need to adapt to oblique wave incidence before showing any migration rate; secondly $c_m(\lambda_{ini.})$ only conveys significance while this lengthscale is dominant. When λ_{final} becomes dominant, $c_m(\lambda_{ini.}) \rightarrow c_m(\lambda_{final})$, in general.

[70] In order to see how $c_m(\lambda_{ini.})$ and $c_m(\lambda_{final})$ compare to c_m for the undisturbed scenario (see Figure 5), these quantities are plotted in Figure 16 for a range of $\lambda_{ini.}$. In general, both $c_m(\lambda_{ini.})$ and $c_m(\lambda_{final})$ correspond well with the undisturbed migration rate of the same lengthscales (Figure 16). $c_m(\lambda_{final})$ is generally slightly under-predicted compared to the undisturbed migration rate, however, there is no obvious dependence of $c_m(\lambda_{final})$ on $\lambda_{ini.}$ (note the scale difference between Figures 16a and 16b). Finally, results for different values of $A_{ini.}$ are very similar (not shown), suggesting that the migration rate of both $\lambda_{ini.}$ and λ_{final} are independent of $A_{ini.}$. As mentioned in section 4.3, the final equilibrated, finite amplitude of crescentic bed-forms is not only composed of λ_{final} but also of higher-harmonic lengthscales.

[71] Figure 17 shows the alongshore appearance of the crescentic bed patterns at different times (note that results correspond with the case presented in Figures 6b and 6e). Initially bed patterns are sinusoidal, but with time they become asymmetrical. This is caused by amplitude dispersion, as the bed-forms propagate alongshore under oblique incidence and steepen. The result can be seen in the Fourier analysis as a higher harmonic wave ($2k_{final}$) in Figure 6e. Such higher harmonic modes therefore appear to be bound, morphodynamic waves that propagate at $c_m(\lambda_{final})$. However, $c_m(\lambda < \lambda_{final})$ (Figure 16a, right of the dashed lines) $\approx$ $c_m(\lambda_{final})$ (i.e. the waves are approximately non-dispersive in wave number), and it cannot be confirmed by the present results whether these higher harmonic modes propagate at $c_m(\lambda_{final})$ or $c_m(\lambda_{final}/2)$.

4.6. Interaction Between Multiple Pre-Existing Bed-Forms

[72] In reality, a range of different crescentic bed pattern lengthscales will generally be present in the same area [*van*

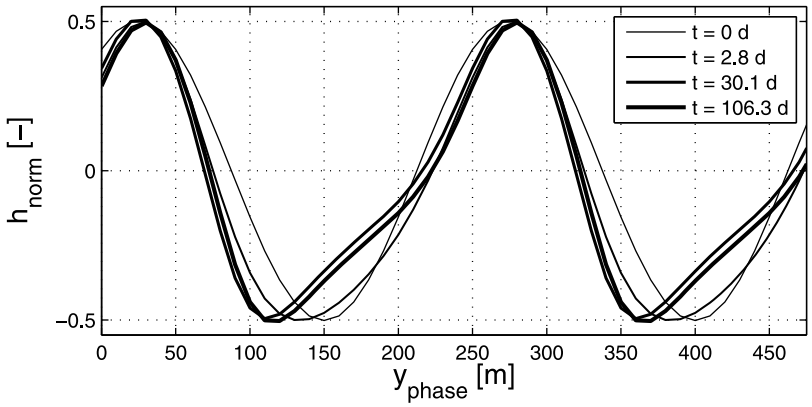

Figure 17. The change in shape for oblique wave incidence bed-forms at the alongshore transect over time (please note that the perturbation profiles are normalized and phase shifted).

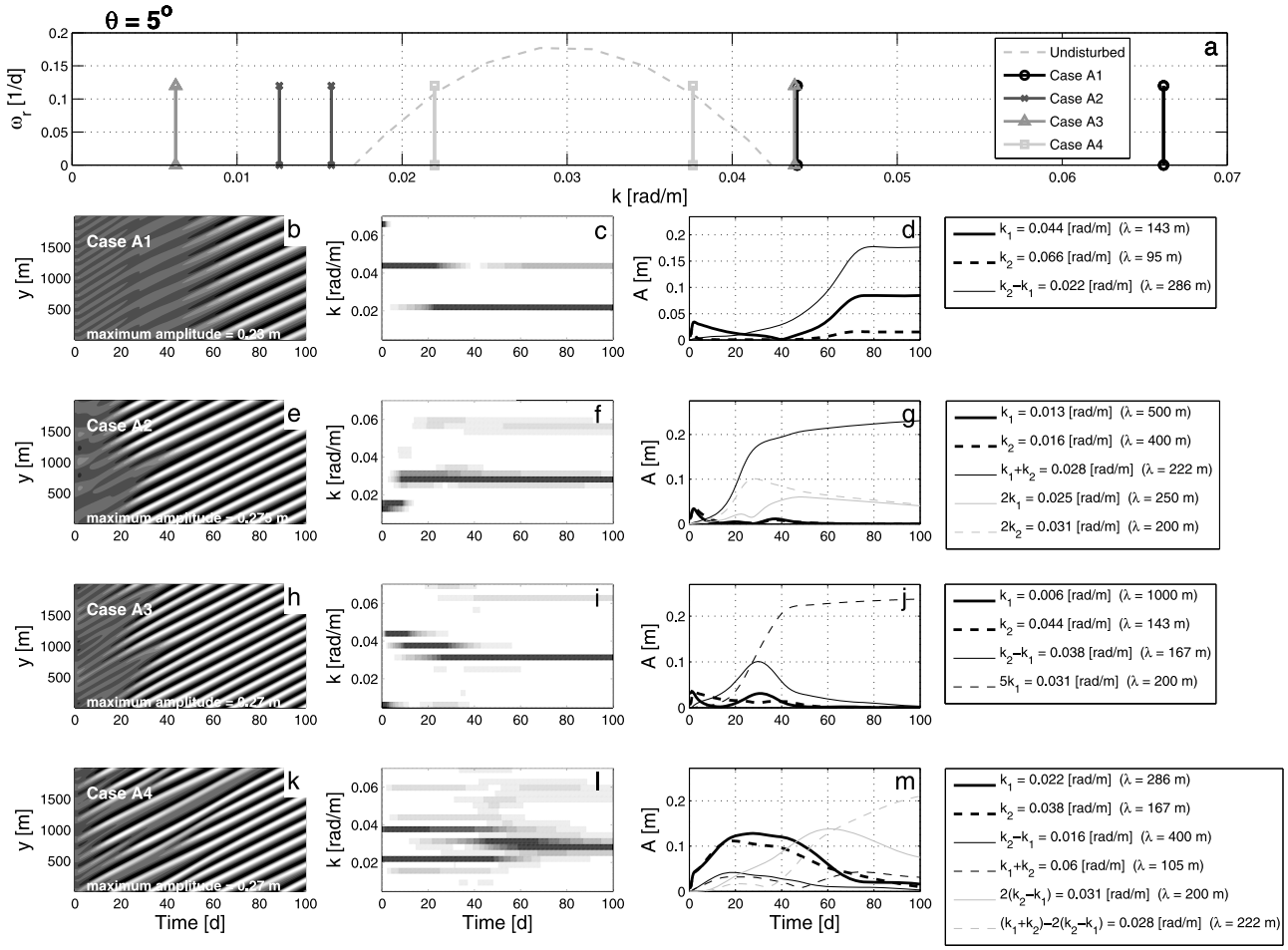

Figure 18. Development of crescentic bed-forms, when two different crescentic bed-forms already exist. (a) Different pre-existing lengthscales (solid lines) ($k = \frac{2\pi}{\lambda}$), along with undisturbed linear growth rate (grey dashed curve). (b–d) Case A1: λ_1 = 143 m, λ_2 = 95 m (k_1 = 0.044, k_2 = 0.066 [rad/m]). (e–g) Case A2: λ_1 = 500 m, λ_2 = 400 m (k_1 = 0.013, k_2 = 0.016 [rad/m]). (h–j) Case A3: λ_1 = 1000 m, λ_2 = 143 m (k_1 = 0.006, k_2 = 0.044 [rad/m]). (k–m) Case A4: λ_1 = 286 m, λ_2 = 167 m (k_1 = 0.022, k_2 = 0.038 [rad/m]). Figures 18b, 18e, 18h, and 18k show evolution of alongshore transect (x = 50 m) of bed profile (white areas crests, black troughs). Figures 18c, 18f, 18i, and 18l show development of dominant lengthscale. Figures 18d, 18g, 18j, and 18m show amplitude development of initial and finally dominant lengthscales and other lengthscales.

Enckevort et al., 2004]. The interaction between pre-existing bed-forms has so far been omitted from the presented work. Here, we investigate the possibility of interaction between different co-existing pre-existing lengthscales, and to what extent these interactions alter the subsequent development of crescentic bed patterns.

[73] The co-existence of two different pre-existing lengthscales ($\lambda_1(k_1)$ and $\lambda_2(k_2)$) can cause new, distinct lengthscales to arise as a result of interaction between the pre-existing lengthscales, at sum or difference wave numbers ($k_{\text{final}} = k_1 + k_2$, or $k_{\text{final}} = k_1 - k_2$). If one of these interacting modes shows significant linear growth in the undisturbed scenario, this lengthscale might become dominant, and overwhelm other modes.

4.6.1. Multiple Bed-Forms of Equal Amplitude

[74] To investigate this behavior, four cases are presented (see Figure 18a). In case A1, two short pre-existing bed-forms are investigated (λ_1 = 143 m, λ_2 = 95 m (k_1 = 0.044 [rad/m], k_2 = 0.066 [rad/m])). Both pre-existing lengthscales decay, and so do higher harmonic lengthscales of both $\lambda_{\text{ini.}}$-values. However, due to mode interaction λ_{final} = 286 m ($k_{\text{final}} = k_2 - k_1$ = 0.022 [rad/m]) arises (Figure 18c). This lengthscale is significantly longer than either pre-existing bed-pattern and shows significant linear growth in the undisturbed case. This newly arising bed pattern develops quickly before reaching a stable situation (Figure 18d). Note, however, that three modes, $k_2 - k_1$, k_1 and k_2 ultimately co-exist and equilibrate, with the difference mode dominant. The presence, at the final stage, of modes other than the finally dominant mode might be the result of the aforementioned bound modes, which arise as the bed-form migrates and steepens.

[75] In case A2 (Figures 18e–18g), two decaying, long, pre-existing lengthscales are implemented (λ_1 = 500 m, λ_2 = 400 m (k_1 = 0.013 [rad/m], k_2 = 0.016 [rad/m])). The development of either pre-existing bed-form individually

would result in the dominance of a higher harmonic of the pre-existing lengthscale (see Table 2). However, due to interaction between the two pre-existing modes ($k_{final} = k_1 + k_2 = 0.028 \equiv k_{FGM}$ [rad/m], $\lambda_{final} = 222$ m) the undisturbed *FGM* develops, dominating the development of higher harmonics, which also initially develop.

[76] Higher harmonics also affect the crescentic bed-pattern development presented in case A3 (Figures 18h–18j), where both a short and a long, decaying, pre-existing mode are implemented ($\lambda_1 = 1000$ m, $\lambda_2 = 143$ m ($k_1 = 0.006$ [rad/m], $k_2 = 0.044$ [rad/m])). The difference mode ($k_2 - k_1 = 0.038$ [rad/m], $\lambda = 167$ m) only shows limited linear growth, and only remains dominant for a brief period, before being overwhelmed by a faster growing mode resulting from interaction of λ_1 harmonics ($k_{final} = 5k_1 = 0.031$ [rad/m], $\lambda_{final} = 200$ m). Therefore, the initial amplitude increase due to interaction of two lengthscales can be bigger than that due to (higher harmonic) self-interaction of a single lengthscale, but the subsequent development can still be overwhelmed by a higher harmonic closer to λ_{FGM}.

[77] More complex interactions occur when two pre-existing lengthscales with significant linear growth are implemented (Case A4: $\lambda_1 = 286$ m, $\lambda_2 = 167$ m ($k_1 = 0.022$, $k_2 = 0.038$ [rad/m])). Both pre-existing modes show similar linear growth in the undisturbed scenario, and would develop and reach a stable situation if they were implemented individually (see Figure 7 and Table 2). However, when implemented as co-existing modes, neither reaches a stable situation. Initially, the pre-existing modes develop and are dominant (see Figure 18i). During this period only first-order interacting modes arise: $k_1 + k_2 = 0.06$ [rad/m], $k_2 - k_1 = 0.016$ [rad/m], $2k_1 = 0.044$ [rad/m] and $2k_2 = 0.076$ [rad/m] (the latter not shown in this plot). All these interacting modes, however, decay in the undisturbed scenario. A second-order interacting mode subsequently develops ($2(k_2 - k_1) = 0.031$ [rad/m]) and is briefly dominant, before a third-order mode with an even bigger undisturbed linear growth rate develops ($(k_1 + k_2) - 2(k_2 - k_1) = 0.028$ [rad/m] ($\lambda = 222$ m)), and the bed finally starts to equilibrate.

4.6.2. Variation of Initial Amplitudes

[78] We examine the impact of variation of $A_{ini.}$ for both modes (but for sum of the amplitudes kept constant at 0.15 m; see Figure 19b). One case is examined ($\theta = 5°$, $\lambda_1 = 500$ m ($k_1 = 0.013$ [rad/m]), $\lambda_2 = 133$ m ($k_2 = 0.047$ [rad/m]); note that these settings are different from those shown in Figure 18). Both $k_{ini.}$ decay and higher harmonic mode ($2k_1$), and interacting mode ($k_2 - k_1$) show similar linear growth in the undisturbed scenario (see Figure 19a).

[79] By varying the pre-existing amplitudes, three different modes of development can be observed (see Figure 19c). With $A_1 = 0$ m, bed-pattern development occurs as a result of background noise and λ_{FGM} develops (Case B1); with a small increase in A_1 (Case B2), background noise becomes completely overwhelmed by the development of the interacting mode ($k_2 - k_1$), confirming the very limited impact that background noise can sometimes have on crescentic bed-pattern development, when bed-forms pre-exist. The interacting mode remains dominant up to and including Case B6, when the contribution of the higher harmonic of k_1 ($2k_1$) also becomes significant for a portion of the development (Figure 19i). With a further increase of A_1 (and decrease of A_2), the finally dominant mode becomes $2k_1$ (Case B7).

[80] When crescentic bed-forms with different lengthscales initially co-exist, the pre-existing amplitude significantly impacts the subsequent development of crescentic bed-forms.

[81] The presence of more than one pre-existing mode, therefore, has a significant impact on the subsequent development of bed-forms. Even pre-existing modes that would remain if occurring individually, can give rise to bed-forms with different lengthscales, if more than one mode pre-exists. All interactions seem, however, to be governed by the undisturbed linear growth rate curve, with all developing bed-forms having increased linear growth rates, compared to the pre-existing modes.

5. Relation to Crescentic Bars in the Field

[82] Various points must be considered when attempting to put model results presented here into context with field observations. Firstly, so far only the impact of monochromatic (or bichromatic) bathymetric perturbations have been studies. A more realistic beach state is likely to contain multiple pre-existing bed-forms.

[83] Secondly, when comparing model predictions with field observations, the impact of pre-existing bed-forms must be included in the analysis.

5.1. Pre-Existing Bed-Forms in a Linear Stability Analysis

[84] Presented results show that non-linear evolution from a periodically disturbed beach profile can partially be described using only a linear stability analysis. Finally dominant lengthscales are always near the peak of the undisturbed growth rate curve (as obtained from a linear stability analysis). Final amplitudes show little dependence on initial lengthscales. There is, however, strong agreement between ω_r- and c_m-values and values from linear theory, for both growing and decaying bed-forms.

[85] All this suggests that for crescentic bed-forms under real-world circumstances, a linear stability analysis would be sufficient, in principle, to give an accurate prediction of subsequent development after, for instance, a change in wave conditions.

[86] However, this analysis should be implemented in a different way than has been done previously [*Tiessen et al.*, 2010]; the entire growth rate curve should be considered, not only the *FGM*, along with higher harmonic generation and, if several different pre-existing lengthscales co-exist, their interaction. Note, however, that a strong proviso on this is that the wavefield should not be significantly directionally spread [*Reniers et al.*, 2004; *MacMahan et al.*, 2006]. In reality, forcing conditions are never stable in time, and this will cause interruptions in bed pattern development. A sequence of different forcing conditions will initiate the development of different lengthscales [*van Enckevort et al.*, 2004].

[87] Considering such a (hypothetical) sequence of events, starting from an alongshore constant beach, mild forcing conditions will cause short linearly growing modes around the undisturbed fastest growing mode to develop. If the forcing conditions subsequently become more energetic,

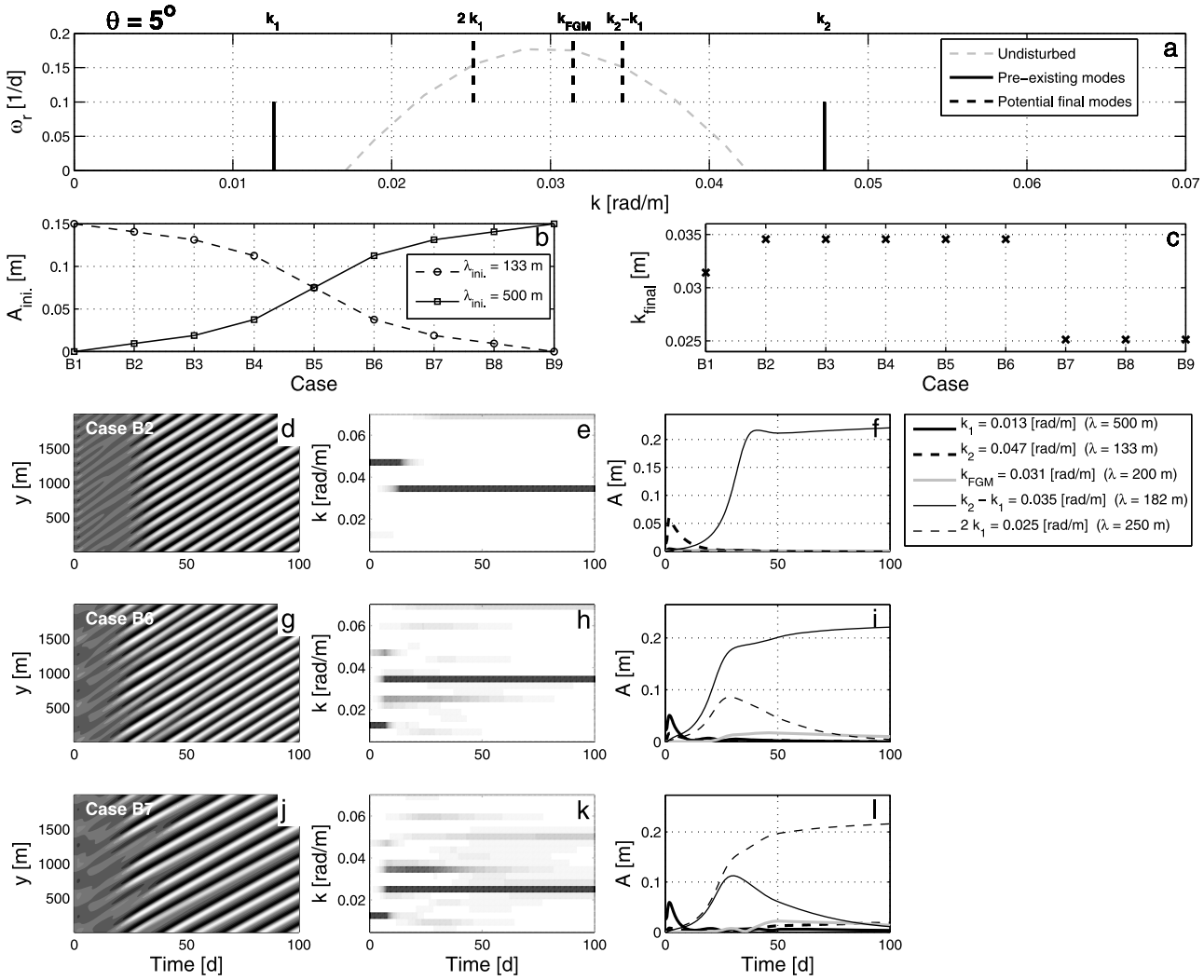

Figure 19. Effect of different pre-existing amplitudes when two pre-existing bed-forms co-exist. (a) Pre-existing modes (solid black lines) and potentially developing lengthscales (dashed black lines), with undisturbed growth rate (dashed grey line, scale on left). (b) Examined pre-existing amplitude combinations; N.B. sum of amplitudes constant (0.15 m). (c) Finally dominant lengthscale for different cases (N.B. cases here are different from those of Figure 18). (d–f) Cases B2 (A_1 = 0.0094 m, A_2 = 0.14 m), (g–i) B6 (A_1 = 0.11 m, A_2 = 0.038 m) and (j–l) B7 (A_1 = 0.13 m, A_2 = 0.019 m) shown in more detail. Figures 19d, 19g, and 19j show evolution of alongshore bed profile (white areas crests, black troughs). Figures 19e, 19h, and 19k show evolution of dominant lengthscale. Figures 19f, 19i, and 19j show amplitude development of initial and finally dominant bed pattern lengthscales and other lengthscales.

longer bed-forms will develop. Our results suggest that these newly arising bed-forms will not depend on the existing bed-forms, but will instead develop from background noise, with the newly established lengthscale being the new undisturbed fastest growing mode.

[88] These longer bed-forms will themselves subsequently break-up if subsequent, moderate forcing conditions were then to occur. A higher harmonic of the pre-existing lengthscale would probably develop subsequently, assuming that the bed-forms created under the initial forcing conditions had been removed completely. If after the second set of wave conditions, bed-forms from both the first two scenarios were to co-exist to some degree, it is possible that this will lead to development of an interacting mode.

[89] Note that k_{final} for one set of forcing conditions is not unique, and depends on the previous forcing conditions and bathymetry.

[90] In order to predict the development of crescentic bed-forms as observed in the field, the bathymetric state of the examined beach at the start of the run must be known. The initial starting position of such a model run would be where an initial amplitude is defined for all examined lengthscales. Argus imaging data alone is probably insufficient, since this can only give a quantitative description of the crescentic bed-pattern lengthscale but not the amplitude. A potential starting position for the comparison between model predictions and field observations might be immediately post-storm, when it can be assumed that all bed-forms are wiped

out, and the amplitudes of the examined lengthscales are small.

5.2. Pathway for Field Data Analysis

[91] In many field observations, the observed crescentic bed pattern lengthscale or rip spacing is used as a characteristic of the bathymetric state, and used for comparison with forcing conditions. However, findings generally suggest only limited correspondence with wave height characteristics. *van Enckevort et al.* [2004] suggest a positive correlation between wave height and bed pattern lengthscale at Duck (USA), Miyazaki (Japan) and the Gold Coast (Australia). However, *Lafon et al.* [2005] observed an opposite relation at Truc Vert beach in France. Recently, both *Holman et al.* [2006] and *Turner et al.* [2007] suggest that a relationship between wave height and crescentic bed pattern lengthscale cannot be observed.

[92] Although modeling results (starting from an alongshore constant bed) sometimes suggest a strong relationship between wave height and bed-pattern length scale, other wave characteristics, such as wave period and wave angle, can be important in this regard [*Deigaard et al.*, 1999; *Ribas et al.*, 2003; *Calvete et al.*, 2005]. Furthermore, saturation can sometimes render the wave height/spacing relation void [see *Calvete et al.*, 2005]. *Tiessen et al.* [2010] showed that not only is the bed pattern lengthscale affected by forcing conditions, but so is the (linear) growth rate, and therefore the likelihood of significant bed pattern development. It might therefore be more appropriate to identify forcing conditions that contribute most to the development of crescentic bars, before comparing forcing conditions with field observations. The effects of directional spreading of the wavefield [*Reniers et al.*, 2004] could further contribute to obscuring a direct relation between wave height and crescentic bed pattern lengthscale.

[93] *Holman et al.* [2006] examined the relation between bar-to-shore distance and bed pattern lengthscale [see also *Deigaard et al.*, 1999; *Damgaard et al.*, 2002]; however, changes in bar height and onshore and offshore beach gradient can have significant contributions as well [see *Calvete et al.*, 2007]. Tidal variation can also, in theory, affect crescentic bed pattern lengthscale and (linear) growth rate [see *Tiessen et al.*, 2010], and this could be significant, causing substantial variation in local forcing conditions.

[94] In the field, the pre-existing bed-forms have been suggested to have a significant impact [*Turner et al.*, 2007]; in this paper, modeling results also point to their importance. Even when, during a storm, bed patterns are wiped out, small remaining perturbations can cause the bed to evolve differently (see Figure 19d, where Case B2 shows that an initial amplitude of only 1 cm for one of the modes causes a completely different bed pattern to develop).

[95] To account for pre-existence of bed-forms, results presented here could be a tool for identifying potential interaction between pre-existing modes and other driving forces for bathymetric evolution, such as forcing conditions. As noted previously, longer pre-existing length scales can relatively easily be transformed into shorter bed-forms, due to higher harmonic interaction; shorter bed-forms potentially remain dominant over longer periods of time, since the development of longer bed-forms has to start from background noise. This was to a certain extent observed in reality by *van Enckevort et al.* [2004], who showed that immediately post-storm longer bed-forms evolved, which subsequently were broken up into shorter bed patterns, within the next couple of days. The lengthscale of these bed-forms did subsequently not change until a new storm would (largely) remove all pre-existing bed-forms. The amplitude of pre-existing bed-forms has only limited impact on the bathymetric evolution. However, changing forcing conditions will cause frequent changes in the bathymetric development. Larger pre-existing modes will therefore be more likely to remain, especially when pre-existing modes generally lie within the positive part of the undisturbed growth rate curve.

6. Discussion

[96] The aim of this research was to observe specific behavior that is related to the effects of pre-existing bed-forms. As a result, many conditions were idealized to create circumstances causing only gradual evolution of bed-forms.

6.1. Down-Slope Term

[97] The results presented so far suggest that there can be a long period of time before a bed-form breaks up or merges. The model runs were carried out using a high down-slope term ($\gamma = 5$ [m^2/s]). This value has been used before by *Garnier et al.* [2008] to create circumstances that result in numerically stable model runs. However, this value does not necessarily describe accurately the speed at which bed patterns form. Model results show, therefore, a much more gradual development than would be observed in reality (observed, for instance, by *van Enckevort et al.* [2004]). Characteristic times, such as when the dominant bed pattern lengthscale changes, are therefore not directly comparable with reality.

6.2. Weak Non-Linearity

[98] A second concern related to the big down-slope term is the potentially limited non-linearity within the model. By increasing γ, undisturbed linear growth rates are reduced, and in this case only a small range of bed pattern lengthscales shows linear growth (see Figures 20c, 20f, 20i, 20l, and 20o). This has the advantage that pre-existing bed patterns that decay in the undisturbed case can also be investigated; application of a smaller down-slope term (1.6 [m^2/s]) leads to linear growth across the entire range of crescentic bed pattern lengthscales. However, the increased value of γ also means that the results presented in this paper could potentially be the results of only weakly non-linear interactions, when the true dynamics are expected to be strongly non-linear.

[99] To see the impact of different γ-values on the development of the bathymetry when bed patterns pre-exist we present Figure 20. Smaller down-slope terms result in a more rapid development, along with an increased final amplitude. The Fourier analysis of the alongshore transect shows that small γ-values result in an increased development of higher harmonics, along with increased interactions between them. However, the different finally dominant lengthscale of $\frac{\lambda_{ini}}{3}$ (166 m, $k = 0.038$ [rad/m]) for small down-slope terms ($\gamma = 1.6, 2, 3$ [m^2/s]) compared to $\frac{\lambda_{ini}}{2}$ (250 m, $k = 0.025$ [rad/m]) can be explained as the result of a shift of the undisturbed *FGM* toward a smaller lengthscale. The

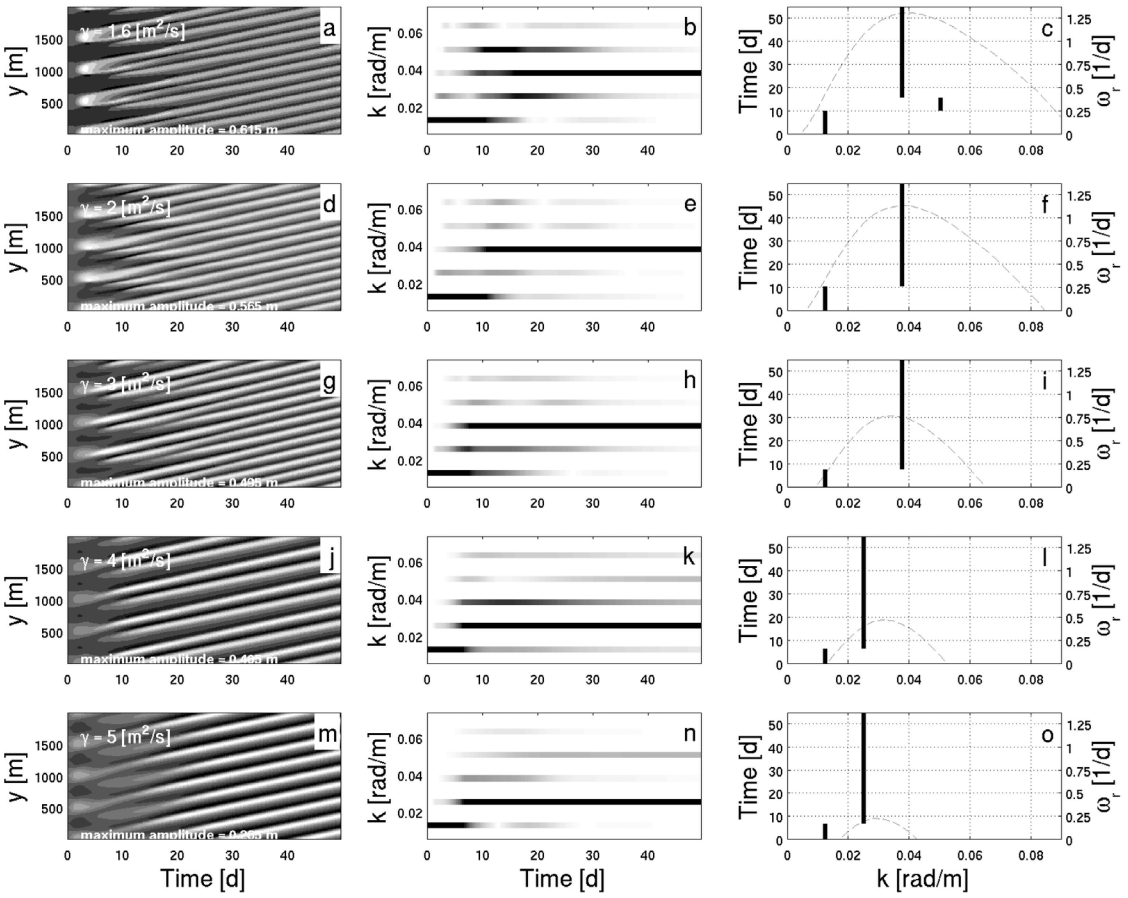

Figure 20. Impact of different down-slope term (γ) values on development of bathymetry when bed patterns pre-exist ($\lambda_{ini.}$ = 500 m, $A_{ini.}$ = 0.15 m). (a–c) γ = 1.6 [m^2/s], (d–f) γ = 2 [m^2/s], (g–i) γ = 3 [m^2/s], (j–l) γ = 4 [m^2/s], (m–o) γ = 5 [m^2/s]. Figures 20a, 20d, 20g, 20j, and 20m show bathymetric evolution of alongshore transect. Figures 20b, 20e, 20h, 20k, and 20n show development of dominance of different lengthscales over time. Figures 20c, 20f, 20i, 20l, and 20o show dominant lengthscale evolution (thick black line, scale on left) along with undisturbed growth rate curve (dashed grey line, scale on right).

only other difference is due to the larger growth rate of $k_{ini.}$ (and all other lengthscales), which, however, results in only a limited difference in the subsequent development (e.g. slightly longer period of dominance of $k_{ini.}$). Ultimately, regardless of γ, the same harmonics are excited and λ_{final} is governed by $\lambda_{ini.}$ and its relation to the undisturbed growth rate curve.

[100] Also note that for smaller values of γ, the span of the linear growth rate curve is increased and more lengthscales show linear growth (even leading to $\lambda_{ini.}$ showing linear growth for $\gamma < 3$ [m^2/s]). As can be seen in Figure 20, even when the pre-existing lengthscale displays significant linear growth, it still become overwhelmed by a lengthscale with a bigger linear growth rate. This development of the bathymetry shows similarities with the behavior observed for pre-existing lengthscales at the edge of the linear growth rate curve, as discussed in section 4.3. This suggests that the development of the bathymetry when pre-existing bed patterns are present, does not depend on whether the pre-existing lengthscale shows linear growth or decay in the undisturbed scenario, but is related to the relative growth rate compared to $\omega_r(\lambda_{FGM})$.

6.3. Periodic Boundaries

[101] Periodic alongshore boundaries result in a finite number of lengthscales that can develop within model runs. Only bed-forms that form a factor of the total width of this stretch of beach (2000 m) can be implemented as pre-existing bed-forms and can develop into a finally dominant length scale.

[102] The application of moderate wave conditions, however, results in the development of finally dominant lengthscales that are reasonably short (λ_{FGM} = 166 m ($\theta = 0°$) and λ_{FGM} = 200 m ($\theta = 5°$)), and the range of possible lengthscales in that region is large enough to give reliable predictions of the finally dominant lengthscale. Experiments with an extended domain length (3333 m) reveal the same bathymetric evolution and result in almost exactly the same mode development, suggesting that results presented here are robust to variations in domain boundaries.

6.4. Pre-Existing Bed-Forms Derived From Linear Stability Model Output

[103] The pre-existing bed-forms used as initial bathymetries in our simulations do not correspond exactly with

solutions of our morphodynamical system, hence the aforementioned initial onshore adjustment.

[104] Note also that morphologies derived from a linear stability analysis (Morfo60) and which are ascribed finite amplitudes will never correspond exactly to valid solutions in a fully non-linear system. Research in this area suggests that bed-forms not only grow in height but also become asymmetric, for instance the rip-channels become more narrow and the bar crests migrate shoreward [*Ranasinghe et al.*, 2004; *MacMahan et al.*, 2006; *Garnier et al.*, 2010].

[105] The appearance of the pre-existing bed-forms also has relevance in a comparison with the approach taken by *Smit* [2010], who, as mentioned, applied two sets of wave conditions in sequence. The degree to which the first morphology is "out of kilter" with the second depends on the speed of transition between the two sets of wave conditions. Nonetheless, we have investigated amplitude development from initial morphologies that correspond more closely to valid solutions; amplitude development shows no significant differences (not shown). Secondly, the aforementioned initial shoreward adjustment, observed for Morfo60 pre-existing bed-forms, gives a strong indication that initial discrepancies are soon accounted for in the model development.

[106] Our experiments suggest that regardless of the difference between the initial morphology (and therefore the implied previous wave conditions) and the ensuing wave conditions, the final morphology will be governed primarily by the undisturbed growth rate curve in the ensuing wave condition, and also by the dominant wavelength of the existing morphology.

6.5. Co-Existence of a Range of Pre-Existing Lengthscales

[107] We have examined monochromatic pre-existing bed-forms, and some examples of interaction of multiple modes. However, in the field a continuous spectrum of lengthscales is generally observed [*van Enckevort et al.*, 2004], implying excitation of a wider range of lengthscales.

[108] Runs that included random perturbations imposed on pre-existing bed-forms, and which therefore excite a wider range of lengthscales (not shown here), show that although a wider range of lengthscales develops, the finally dominant lengthscale does not change.

6.6. The Development of Characteristic Lengthscales

[109] We have focused here on the amplitude development of $\lambda_{ini.}$ and λ_{final}. In general, the modeled development of crescentic bed patterns can accurately be described by these two lengthscales alone. During relatively brief durations, other lengthscales can also have a significant contribution, for instance, the development of higher harmonic of $\lambda_{ini.}$ (for $\lambda_{ini.} \gg \lambda_{FGM}$), (see, e.g., Figure 6d).

[110] However, the occurrence of other lengthscale developments is generally brief, and only has limited impact on the overall development, suggesting that the characteristics identified in this research accurately capture the overall development.

6.7. The Alongshore Transect

[111] The position of the alongshore transect at which these characteristic amplitudes have been determined, is not in general the position of the biggest amplitude in the domain. This is generally (after an initial start up period of 2 days) around 5 to 10 m further offshore. However, the behavior observed at the maximum amplitude closely corresponds with that of the chosen alongshore transect. The chosen transect therefore gives a good representation of the occurring processes.

6.8. Development Toward a New Stable State

[112] The linear growth rate is used in this paper to quantify the initial response of the system to the pre-existence of bed patterns. However, how a bed-form reaches its final height, and the process of saturation of the growth prior to this occurrence is not quantified here. Recent investigations into this have identified and quantified different processes occurring during these stages of development [*Garnier et al.*, 2010]. The final development of crescentic bed-forms, when pre-existing bed-forms occur, shows close correspondence with the development starting from an alongshore constant beach. Secondly, both the saturation of the linear growth [*Garnier et al.*, 2010], and final amplitude of λ_{final} correspond closely with the development of bed-forms that do not break-up or merge (see Figure 9), suggesting that the final stages of bed-pattern development are not influenced by the pre-existence of crescentic bed patterns.

7. Conclusions

[113] 1. Pre-existing bed-forms remain when their lengthscale shows significant undisturbed linear growth. Non-linear simulations of the evolution of the nearshore seabed, with crescentic bed-forms implemented at the start of the run, show that pre-existing bed patterns with a lengthscale that is close to the dominant lengthscale of the undisturbed case (λ_{FGM}) will undergo further growth and reach a final height within a short period of time. Initial lengthscales that are outside the linear growth rate curve of the undisturbed development will decay, and crescentic bed patterns with lengthscales close to λ_{FGM} will develop. The existence of pre-existing bed-forms makes it necessary to interpret the predictions made by a linear stability analysis with care. Not only must the linear fastest growing mode be considered (as was done by *Tiessen et al.* [2010]), but also a wider array of growing bed-patterns, when determining the subsequent bathymetric development when bed-forms pre-exist.

[114] 2. If $\lambda_{ini.} \gg \lambda_{FGM}$, the newly arising lengthscale is a higher harmonic of $\lambda_{ini.}$ For a mode for which $\lambda_{ini.} \ll \lambda_{FGM}$, $\lambda_{ini.}$ will almost completely disappear before a bed-form at λ_{FGM} develops. This development generally takes a long time, since the newly developing bed-form arises from the background noise and is not directly excited by the pre-existing bed-form. A long, decaying, pre-existing bed pattern ($\lambda_{ini.} \gg \lambda_{FGM}$) breaks up much more quickly, not because the decay rate is higher, but because the higher harmonics (initially $2k_{ini.}$, but also others) will in general possess positive growth rates (or at least much smaller decay rates); the finally dominant lengthscale (λ_{final}) is then generally a factor of $\lambda_{ini.}$, with λ_{final} closer to λ_{FGM} than is $\lambda_{ini.}$. Note, however, that, crucially, the finally dominant lengthscale is not necessarily the harmonic closest to λ_{FGM}, but merely one that possesses a significant growth rate compared to $\omega_r(k_{FGM})$ and that is sufficiently excited by harmonic (self)-interaction.

[115] 3. An increase of $A_{ini.}$ results in more rapid development toward a new stable situation. Either if $\lambda_{ini.} = \lambda_{final}$, or when $\lambda_{ini.} \gg \lambda_{final}$, energy is fed from $\lambda_{ini.}$ into λ_{final} due to higher harmonic interaction, or when $\lambda_{ini.} \ll \lambda_{final}$ due to background noise. Secondly, increased $A_{ini.}$ result in increased duration before dominance changes from $\lambda_{ini.}$ to λ_{final}. No direct effect from $A_{ini.}$ on λ_{final} is observed in these results. However pre-existing lengthscales that grow very gradually might remain dominant when $A_{ini.}$ is big, whereas if $A_{ini.}$ is small these pre-existing bed-forms will become overwhelmed by lengthscales closer to λ_{FGM}.

[116] 4. The undisturbed behavior governs the linear growth rate and migration when pre-existing modes occur. The rate of linear growth and decay of the pre-existing bed-forms as well as that of the finally dominant bed pattern closely corresponds with the undisturbed linear growth rate curve. The duration of linear growth is dependent on the amplitude of the finally dominant bed-form, as well as their linear growth rate. No linear growth can be observed for large pre-existing modes close to λ_{FGM}. Neither $A_{ini.}$ nor $\lambda_{ini.}$ affects the migration rate of the finally dominant mode significantly. The migration rates observed during periods of dominance of both the pre-existing and the newly arising bed-forms closely correspond with those observed when starting from an alongshore constant beach.

[117] 5. Multiple co-existing pre-existing modes cause mode-interaction. The presence of more than one pre-existing bed pattern lengthscale can result in the development of bed patterns at sum or difference wave numbers by the interaction between these pre-existing modes. Whether a higher harmonic or the interacting mode of both pre-existing lengthscales forms, depends on the undisturbed linear growth rates of the lengthscales involved. When pre-existing modes of different amplitude co-exist, the different initial amplitude of these modes can also significantly influence the final appearance of the bed-forms. Either a higher harmonic develops of one of the pre-existing modes, or an interacting mode of both pre-existing lengthscales can develop, depending on the relative amplitude of both pre-existing bed-forms. This situation will be further complicated if the relevant higher harmonic and the sum or difference modes possess different growth rates.

[118] 6. Pre-existing bed-forms can significantly influence the development of crescentic bed-forms. In order to describe subsequent nearshore bathymetric evolution, knowledge of the undisturbed crescentic bed pattern development is essential, but both the initial lengthscale as well as the initial amplitude are important. The pre-existing lengthscale is crucial for the determination of the finally dominant lengthscale, as well as the development time before a new stable situation is reached, and also the mechanism by which it is reached. The initial amplitude affects this development time as well, since bigger initial amplitudes will accelerate the process of formation. The extent to which the initial morphological response of these pre-existing bed-forms can be described by linear equations (e.g. linear stability analysis) is dependent on the initial amplitude; increased initial amplitudes result in a more non-linear response and therefore a reduced accuracy of linear stability predictions. In the presence of multiple pre-existing modes, the different lengthscales and amplitudes of these modes are important for the determination of the subsequent development, and the evolution toward a final stable mode.

[119] **Acknowledgments.** Meinard Tiessen gratefully acknowledges the support of the UK Engineering and Physical Sciences Research Council (EPSRC) under grant EP/P00389/1, the University of Nottingham, and the NIOZ Royal Netherlands Institute for Sea Research during his PhD and past and present post-doctoral positions. The work of Roland Garnier was supported by the University of Nottingham and by the Spanish government through the CTM2006-08875/MAR project and through the "Juan de la Cierva" program.

References

Arifin, R. R., and A. B. Kennedy (2011), The evolution of large scale crescentic bars on the northern Gulf of Mexico coast, *Mar. Geol.*, *285*, 46–58, doi:10.1016/j.margeo.2011.04.003.

Battjes, J. (1975), Modelling of turbulence in the surf zone, in *Modeling 75: Symposium on Modeling Techniques: 2d Annual Symposium of the Waterways, Harbors, and Coastal Engineering Division of ASCE*, vol. 2, pp. 1050–1061, Am. Soc. Civ. Eng., New York.

Blondeaux, P. (2001), Mechanics of coastal forms, *Annu. Rev. Fluid Mech.*, *33*, 339–370.

Bowen, A., and R. Guza (1978), Edge waves and surf beat, *J. Geophys. Res.*, *83*, 1913–1920.

Caballeria, M., G. Coco, A. Falques, and D. A. Huntley (2002), Self-organization mechanisms for the formation of nearshore crescentic and transverse sand bars, *J. Fluid Mech.*, *465*, 379–410.

Calvete, D., N. Dodd, A. Falqués, and S. M. van Leeuwen (2005), Morphological development of rip channel systems: Normal and near-normal wave incidence, *J. Geophys. Res.*, *110*, C10006, doi:10.1029/2004JC002803.

Calvete, D., G. Coco, A. Falqués, and N. Dodd (2007), (Un)predictability in rip channel systems, *Geophys. Res. Lett.*, 34, L05605, doi:10.1029/2006GL028162.

Castelle, B., B. G. Ruessink, P. Bonneton, V. Marieu, N. Bruneau, and T. D. Price (2010), Coupling mechanisms in double sandbar systems. Part 1: Patterns and physical explanation, *Earth Surf. Processes Landforms*, *35*, 476–486.

Coco, G., and A. B. Murray (2007), Patterns in the sand: From forcing templates to self-organisation, *Geomorphology*, *91*, 271–290.

Coco, G., D. A. Huntley, and T. J. O'Hare (2000), Investigation of a self-organization model for beach cusp formation, *J. Geophys. Res.*, *105*, 21,991–22,002.

Damgaard, J. S., N. Dodd, L. J. Hall, and T. J. Chesher (2002), Morphodynamic modelling of rip channel growth, *Coastal Eng.*, *45*, 199–221.

Deigaard, R., N. Drønen, J. Fredsøe, J. H. Jensen, and M. P. Jørgensen (1999), A morphological stability analysis for a long straight barred beach, *Coastal Eng.*, *36*, 171–195.

Dodd, N., P. Blondeaux, D. Calvete, H. E. De Swart, A. Falqués, S. J. M. H. Hulscher, G. Różyński, and G. Vittori (2003), Understanding coastal morphodynamics using stability methods, *J. Coastal Res.*, *19*(4), 849–865.

Falqués, A., G. Coco, and D. A. Huntley (2000), A mechanism for the generation of wave driven rhythmic patterns in the surf zone, *J. Geophys. Res.*, *105*, 24,071–24,087.

Falqués, A., N. Dodd, R. Garnier, F. Ribas, F. MacHardy, L. C. Sancho, P. Larroudé, and D. Calvete (2008), Rhythmic surf-zone bars and morphodynamic self-organization, *Coastal Eng.*, *55*, 622–641, doi:10.1016/j.coasteng.2007.11.012.

Gallop, S. L., K. R. Bryan, G. Coco, and S. A. Stephens (2011), Storm-driven changes in rip channel patterns on an embayed beach, *Geomorphology*, *127*, 179–188, doi:10.1016/j.geomorph.2010.12.014.

Garnier, R. (2006), Nonlinear modelling of surf zone morphodynamical instabilities, Ph.D. thesis, Appl. Physics Dept., Univ. Politècnica de Catalunya, Barcelona, Spain.

Garnier, R., D. Calvete, A. Falqués, and M. Caballeria (2006), Generation and nonlinear evolution of shore-oblique/transverse bars, *J. Fluid Mech.*, *567*, 327–360, doi:10.1017/S0022112006002126.

Garnier, R., D. Calvete, A. Falqués, and N. Dodd (2008), Modelling the formation and the long-term behavior of rip channel systems from the deformation of a longshore bar, *J. Geophys. Res.*, *113*, C07053, doi:10.1029/2007JC004632.

Garnier, R., N. Dodd, A. Falqués, and D. Calvete (2010), Mechanisms controlling crescentic bar amplitude, *J. Geophys. Res.*, *115*, F02007, doi:10.1029/2009JF001407.

Hasan, H., N. Dodd, and R. Garnier (2009), Stabilizing effect of random waves on rip currents, *J. Geophys. Res.*, *114*, C07010, doi:10.1029/2008JC005031.

Hino, M. (1974), Theory on the formation of rip-current and cuspoidal coast, in *Proceedings of the 14th International Conference on Coastal Engineering*, vol. 1, pp. 901–919, Am. Soc. Civ. Eng., New York.

Holman, R., and A. Bowen (1982), Bars, bumps, and holes: Models for the generation of complex beach topography, *J. Geophys. Res.*, *87*, 457–468.

Holman, R. A., G. Symonds, E. B. Thronton, and R. Ranasinghe (2006), Rip spacing and persistence on an embayed beach, *J. Geophys. Res.*, *111*, C01006, doi:10.1029/2005JC002965.

Klein, M. (2006), Modelling rhythmic morphology in the surf zone, Ph.D. thesis, Fac. of Civ. Eng., Delft Univ. of Technol., Delft, Netherlands.

Klein, M. D., and H. M. Schuttelaars (2005), Morphodynamic instabilities on planar beaches: Sensitivity to parameter values and process formulations, *J. Geophys. Res.*, *110*, F04S18, doi:10.1029/2004JF000213.

Klein, M. D., and H. M. Schuttelaars (2006), Morphodynamic evolution of double-barred beaches, *J. Geophys. Res.*, *111*, C06017, doi:10.1029/2005JC003155.

Komar, P. D. (1998), *Beach Processes and Sedimentation*, 2nd ed., 544 pp., Prentice Hall, Upper Saddle River, N. J.

Komar, P. D., and R. A. Holman (1986), Coastal processes and the development of shoreline erosion, *Annu. Rev. Earth Planet. Sci.*, *14*, 237–265.

Lafon, V., H. Dupuis, R. Butel, B. Castelle, D. Michel, H. Howa, and D. De Melo Apoluceno (2005), Morphodynamics of nearshore rhythmic sandbars in a mixed-energy environment (SW France): 2. Physical forcing analysis, *Estuarine Coastal Shelf Sci.*, *65*, 449–462.

Longuet-Higgins, M. S., and R. W. Stewart (1964), Radiation stresses in water waves: A physical discussion with applications, *Deep Sea Res. Oceanogr. Abstr.*, *11*, 529–562.

MacMahan, J., E. B. Thornton, and A. Reniers (2006), Rip current review, *Coastal Eng.*, *53*, 191–208.

Mei, C. C. (1990), *The Applied Dynamics of Ocean Surface Waves*, *Adv. Ser. Ocean Eng.*, vol. 1, 2nd ed., World Sci., Singapore.

Ranasinghe, R., G. Symonds, K. Black, and R. Holman (2004), Morphodynamics of intermediate beaches: A video imaging and numerical modelling study, *Coastal Eng.*, *51*, 629–655.

Reniers, A. J. H. M., J. A. Roelvink, and E. B. Thornton (2004), Morphodynamic modeling of an embayed beach under wave group forcing, *J. Geophys. Res.*, *109*, C01030, doi:10.1029/2002JC001586.

Ribas, F., A. Falqués, and A. Montoto (2003), Nearshore oblique sand bars, *J. Geophys. Res.*, *108*(C4), 3119, doi:10.1029/2001JC000985.

Schielen, R., A. Doelman, and H. de Swart (1993), On the dynamics of free bars in straight channels, *J. Fluid Mech.*, *252*, 325–356.

Smit, M. W. J. (2010), Formation and evolution of nearshore sandbar patterns, Ph.D. thesis, Fac. of Civ. Eng. and Geosci., Delft Univ. of Technol., Delft, Netherlands.

Smit, M. W. J., A. J. H. M. Reniers, B. G. Ruessink, and J. A. Roelvink (2008), The morphological response of a nearshore double sandbar system to constant wave forcing, *Coastal Eng.*, *55*, 761–770.

Soulsby, R. L. (1997), *Dynamics of Marine Sands*, 249 pp., Thomas Telford, London.

Svendsen, I. A. (2006), *Introduction to Nearshore Hydrodynamics*, 722 pp., World Sci., Hackensack, N. J.

Thornton, E. B., and R. T. Guza (1983), Transformation of wave height distribution, *J. Geophys. Res.*, *88*, 5925–5938.

Tiessen, M. C. H., S. M. van Leeuwen, D. Calvete, and N. Dodd (2010), A field test of a linear stability model for crescentic bars, *Coastal Eng.*, *57*, 41–51, doi:10.1016/j.coastaleng.2009.09.002.

Turner, I. L., D. Whyte, B. G. Ruessink, and R. Ratasinghe (2007), Observations of rip spacing, persistence and mobility at a long, straight coast, *Mar. Geol.*, *236*, 209–221.

van Enckevort, I. M. J., and B. G. Ruessink (2003), Video observations of nearshore bar behavior, Part 2: Alongshore non-uniform variability, *Cont. Shelf Res.*, *23*, 513–532.

van Enckevort, I. M. J., B. G. Ruessink, G. Coco, K. Suzukui, I. L. Turner, N. G. Plant, and R. A. Holman (2004), Observations of nearshore crescentic sandbars, *J. Geophys. Res.*, *109*, C06028, doi:10.1029/2003JC002214.

Wright, L. D., and A. D. Short (1984), Morphodynamic variability of surf zone and beaches: A synthesis, *Mar. Geol.*, *56*, 93–118.

Yu, J., and D. N. Slinn (2003), Effects of wave-current interaction on rip currents, *J. Geophys. Res.*, *108*(C3), 3088, doi:10.1029/2001JC001105.

N. Dodd, Faculty of Engineering, University of Nottingham, Nottingham NG7 2RD, UK.

R. Garnier, Instituto de Hidraulica Ambiental, Universidad de Cantabria, ETSI Caminos Canales y Puertos, Avda. los Castros s/n, E-39005 Santander, Spain.

M. C. H. Tiessen, Royal Netherlands Institute for Sea Research, Landsdiep 4, NL-1797 SZ t Horntje, Netherlands. (meinard.tiessen@nioz.nl)